International Journal of
Molecular Sciences

MDPI

Article

The Quest to Quantify Selective and Synergistic Effects of Plasma for Cancer Treatment: Insights from Mathematical Modeling

Charlotta Bengtson * and Annemie Bogaerts

Research Group PLASMANT, Department of Chemistry, University of Antwerp, Universiteitsplein 1, B-2610 Wilrijk-Antwerp, Belgium; annemie.bogaerts@uantwerpen.be
* Correspondence: charlotta.bengtson@uantwerpen.be

Abstract: Cold atmospheric plasma (CAP) and plasma-treated liquids (PTLs) have recently become a promising option for cancer treatment, but the underlying mechanisms of the anti-cancer effect are still to a large extent unknown. Although hydrogen peroxide (H_2O_2) has been recognized as the major anti-cancer agent of PTL and may enable selectivity in a certain concentration regime, the co-existence of nitrite can create a synergistic effect. We develop a mathematical model to describe the key species and features of the cellular response toward PTL. From the numerical solutions, we define a number of dependent variables, which represent feasible measures to quantify cell susceptibility in terms of the H_2O_2 membrane diffusion rate constant and the intracellular catalase concentration. For each of these dependent variables, we investigate the regimes of selective versus non-selective, and of synergistic versus non-synergistic effect to evaluate their potential role as a measure of cell susceptibility. Our results suggest that the maximal intracellular H_2O_2 concentration, which in the selective regime is almost four times greater for the most susceptible cells compared to the most resistant cells, could be used to quantify the cell susceptibility toward exogenous H_2O_2. We believe our theoretical approach brings novelty to the field of plasma oncology, and more broadly, to the field of redox biology, by proposing new ways to quantify the selective and synergistic anti-cancer effect of PTL in terms of inherent cell features.

Keywords: selective cancer treatment; cold atmospheric plasma; hydrogen peroxide; reaction network; mathematical modeling

Citation: Bengtson, C.; Bogaerts, A. The Quest to Quantify Selective and Synergistic Effects of Plasma for Cancer Treatment: Insights from Mathematical Modeling. *Int. J. Mol. Sci.* **2021**, *22*, 5033. https://doi.org/10.3390/ijms22095033

Academic Editor: Akikazu Sakudo

Received: 30 March 2021
Accepted: 6 May 2021
Published: 10 May 2021

1. Introduction

In the last decade, the use of cold atmospheric plasma (CAP), which is an ionized gas near room temperature, has become a novel method to treat cancer. Both direct application of CAP (e.g., by the clinically approved kINPenMED® plasma jet) and indirect treatment by application of plasma-treated liquids (PTLs) have been shown to provide a significant anti-cancer effect [1]. Van Boxem et al. [2] showed that PTLs have an anti-cancer effect for a number of different CAP and liquid conditions, and Lin et al. [3] found that CAP can induce immunogenic cancer cell death. This mode of cell death induced by CAP was later attributed to the CAP generated short-lived reactive species [4]. Moreover, CAP and PTLs have been reported to cause a selective anti-cancer effect [5], although selectivity depends on the cell type, the type of cancer, and the culturing medium [6]. Bekeschus et al. [7] demonstrated, using an *in ovo* model, that CAP is a safe cancer treatment modality with respect to possible metastasis formation. A number of promising results of the clinical application of CAP for cancer treatment have also been published (see e.g., [8,9]).

It is widely believed that the processes leading to cancer cell death are initiated by reactive oxygen and/or nitrogen species (RONS), in particular hydrogen peroxide (H_2O_2), but the knowledge about the specific mechanisms underlying cell death induced by CAP and PTL is still very limited. The lack of understanding of the combined effect of RONS

contained in CAP and PTL in terms of the cellular response to exposure is problematic in the development of CAP/PTL treatment as a standardized cancer therapy for clinical use. Ultimately, it should be possible to predict and quantify the susceptibility to CAP/PTL of a particular cell line in terms of features specifically associated with those cells.

So far, the vast majority of the literature in plasma oncology are experimental studies. As a complement, another approach to increase the understanding of complex biological systems such as the interaction between cells and PTL, is to develop a mathematical model that includes all the known information (of major importance in the given context) about the system and use it to investigate the system's response to various conditions. Especially, the system's response to a perturbation of the "normal" conditions can be analyzed. Furthermore, the development of the mathematical model itself can be seen as a way to summarize the current state of knowledge on the matter in a compact manner; it can be seen as the current "working hypothesis" of the mechanisms and processes governing the system dynamics.

Mathematical modeling has indeed proven to be a useful approach to increase our knowledge about the mechanisms of the cell's antioxidant defense and redox signaling. Some examples are the range of diffusion of H_2O_2 in the cytosol [10,11] and the cellular decomposition of exogenous H_2O_2 [12–14]. In the context of plasma oncology, two catalase-dependent apoptotic pathways associated with cancer cells, which possibly could be reactivated by CAP and thus explain the anti-cancer effect of CAP, have been investigated by mathematical modeling [15]. It was found that these pathways are unlikely to account for the anti-cancer effect of CAP and thus the underlying cause has to be studied further.

In the present study, we develop a mathematical model that includes the species and mechanisms of major importance in the context of a cell system exposed to PTL. The ultimate aim is to find a measure in terms of key features and characteristics of cells, which is able to quantify a particular cell system's susceptibility toward PTL and thus explain differences in response between normal cells and cancer cells. To the best of our knowledge, this is a completely novel approach in the field of plasma oncology, and we believe that our study will provide a new perspective and new insights as a complement to the experimental studies. An extensive summary of the background, leading to the more detailed research question, is provided in Section 2.

2. Experimentally Observed Cytotoxic Effects of CAP and PTL and Possible Features Determining Cancer Cell Susceptibility

An immediate effect of CAP treatment of cancer cells is an increase in intracellular RONS [16–20]. The significance of this RONS accumulation has been verified by the observation that the treatment does not succeed if the cancer cells have been pre-treated with intracellular RONS scavengers [17,21,22]. The origin of the increase in intracellular RONS after CAP treatment is still under investigation, but a hypothesis consistent with experimental observations is that it is caused by a diffusion of extracellular CAP-originated RONS across the cell membrane [17,18,23,24].

It has been demonstrated that the anti-cancer effect of CAP can also be induced by the species in PTL. In PTL, which mainly consists of H_2O_2, NO_2^- and NO_3^- [25–27], H_2O_2 has been shown to be of major importance [2,25–31]. It has been demonstrated that the H_2O_2 consumption rate, which is cell specific, of cancer cells after PTL treatment, is a key factor determining the specific susceptibility of cancer cell lines to PTL. More explicitly, it has been reported that the higher the H_2O_2 consumption rate of cancer cells, the lower the susceptibility toward CAP/PTL [32]. The susceptibility of cancer cells toward exogenous H_2O_2 has also been shown in [33–36]. However, it has been found that H_2O_2 alone cannot account for the total anti-cancer effect observed for PTL [27]. In this context, there are some reports of a synergistic effect of H_2O_2 and NO_2^- in PTL [25,26]. Thus, the cytotoxic effect of H_2O_2 seems to be enhanced in the presence of NO_2^-. The study in [26] found a *selective, synergistic* anti-cancer effect for H_2O_2 in the µM-range and NO_2^- in the mM-range, whereas in [25], a *non-selective, synergistic* anti-cancer effect was reported when H_2O_2 and NO_2^- were both in the mM-range. Since H_2O_2 and NO_2^- in PTL may react to form $ONOO^-$ [37], which

is known to be highly toxic to cells, it has been speculated whether $ONOO^-$ is the species causing the synergistic effect of NO_2^- and H_2O_2. Its formation could thus potentially increase the cytotoxicity of PTL compared to an equal concentration of H_2O_2 only.

To summarize, some key points of the observed cytotoxic effects of CAP or PTL are:

- An intracellular increase of RONS, which is likely to be caused by diffusion of CAP-originated constituents through the cell membrane, is crucial for cell cytotoxicity.
- The key species in the anti-cancer effect of PTL is H_2O_2 (note that this may be different for direct CAP treatment, where short-lived RONS also play a crucial role [4,38]), and the corresponding cytotoxicity is inversely proportional to the extracellular consumption rate of H_2O_2.
- The effect of extracellular H_2O_2 is enhanced in the presence of NO_2^-, which can be a clue to understanding why PTL enables a more efficient treatment than a mock solution of H_2O_2 only.

Thus, from the information presented in literature, we can conclude that the cellular response to an addition of extracellular H_2O_2, with and without a simultaneous addition of NO_2^-, is crucial to understanding the anti-cancer effect of PTL. In Section 2.1, we introduce the key parameters to predict the response toward extracellular H_2O_2 of cells. We also relate this to general differences between normal cells and cancer cells. Based on this information and knowledge, we introduce our approach, and formulate our research question and aim in detail in Section 2.2.

2.1. Differences in Cellular Response to Exogenous Hydrogen Peroxide

In particular, two factors determine whether a certain cell line is susceptible to the exposure of exogenous H_2O_2:

- The plasma-membrane H_2O_2 diffusion rate constant and
- The intracellular expression of catalase.

Several cancer cell lines have shown a common phenotype of *decreased* catalase expression and *increased* aquaporin expression (that facilitates the transport of H_2O_2 through the cell membrane [39–42] and thus determines the H_2O_2 membrane diffusion rate) compared to normal cells. Hence, cancer cells in general can be assumed to be more susceptible to exogenous H_2O_2.

2.1.1. Membrane Diffusion Rate of Hydrogen Peroxide in Normal versus Cancer Cells

Aquaporins are proteins that form pores in the cell membrane. Primarily, they facilitate the transport of water between cells, but they also enable the trans-membrane diffusion of H_2O_2 (due to the chemical similarities between both molecules). Thus, the aquaporin expression in the cell membrane relates to the membrane diffusion rate of H_2O_2. Many aquaporins have been found to be overexpressed in tumors of different origins, especially in aggressive tumors [43]. Since different cancer cell lines express aquaporins to various extents [43,44], the different responses of H_2O_2-exposure by different cancer cell lines can at least partly be explained by the non-identical levels of aquaporin expression. In [45], it was found that aquaporin 3 accounted for nearly 80% of the membrane diffusion of H_2O_2 in a human pancreatic cancer cell line. For cells with a decreased aquaporin 3 expression, the rate of H_2O_2-uptake from the extracellular compartment was significantly decreased. It has furthermore been shown that for glioblastoma tumor cells, the anti-cancer effect of PTL as well as the increase of the concentration of intracellular RONS was significantly inhibited when aquaporin 8 was inhibited [46].

2.1.2. Catalase Activity in Normal versus Cancer Cells

Catalase is one of the main enzymes of the antioxidant defense system of cells of almost all aerobic organisms. The biological role of catalase is to regulate intracellular steady-state concentrations of H_2O_2, and experimental investigations and kinetic models using in vitro data have demonstrated that catalase is the major enzyme involved in the antioxidant

defense against high concentrations of H_2O_2 [12,47–49]. In particular, catalase has been shown to be responsible for the clearance of *exogenous* H_2O_2 in vitro and in vivo [12,50–52].

Although catalase levels vary widely across cell lines, the total concentration of catalase (extracellular and intracellular) is frequently reported to be lower in cancer cells than in normal cells [36,53–60]. In [61], it was found that the catalase activity in various cancer cells is up to an order of magnitude lower compared to normal cells, and in [62], it was shown that normal cells had a better capacity to remove extracellular H_2O_2 than cancer cells; the rate constants for removal of extracellular H_2O_2 were on average two times higher in normal cells than in cancer cells. Furthermore, it was reported in [62] that the rate constants for H_2O_2 removal by different cell lines correlated with the number of active catalase monomers per cell.

However, while in general, the levels of catalase are low in cancer cells, catalase activity appears to vary greatly across different cancer cell lines [63]. In [34], it was found that three cancer cell lines (glioblastoma) that were extremely susceptible to H_2O_2 (generated by ascorbic acid) had reduced activity of intracellular catalase. Ascorbic acid-resistant cancer cell lines, on the other hand, exhibited significantly higher levels of catalase, but catalase knockdown sensitized these cell lines to extracellular H_2O_2.

An additional aspect of catalase that may be of interest in the context of cytotoxicity of CAP and PTL, is that it has been shown to decompose $ONOO^-$ [64]. Thus, if the synergistic effect of H_2O_2 and NO_2^- is to be found in the formation of $ONOO^-$, catalase might have a double function (i.e., as a protective factor toward exogenous exposure of both H_2O_2 and NO_2^-).

2.2. Approach and Research Question

In this study, we develop a mathematical model of the kinetics of the key species of PTL (i.e., H_2O_2 and NO_2^-) as well as of the processes governing the interaction with a cell system, which are given in terms of the H_2O_2 membrane diffusion rate constant and the intracellular catalase concentration. The system modeled is illustrated in Figure 1.

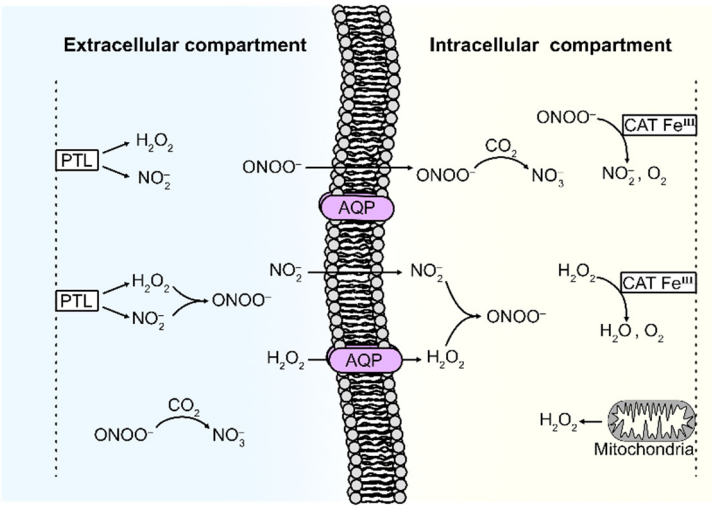

Figure 1. Illustration of the system representing a cell exposed to PTL.

As can be seen, the system consists of two compartments: the extracellular compartment (EC) and the intracellular compartment (IC). The two compartments are separated by the cell membrane, which some species in the system can diffuse through. Our mathematical model is explained in detail in Section 5, with references to all input data and assumptions made. Briefly, it takes into account (i) the diffusion of H_2O_2 and NO_2^- from the EC (where these species are supplied by PTL) to the IC, (ii) the formation of $ONOO^-$ from H_2O_2 and NO_2^- (in both the IC and EC), (iii) the mitochondrial production of H_2O_2 (in the IC), and (iv) the decomposition of H_2O_2 and $ONOO^-$ (in the IC). Furthermore, (v) since

the CO_2-catalyzed consumption is considered to be the main route for $ONOO^-$-decay in biological systems (due to a high CO_2-concentration) [65–69], this reaction is also included.

There have already been attempts to capture the susceptibility toward exogenous H_2O_2 of different cell lines in terms of their H_2O_2 membrane diffusion rate constant and intracellular catalase concentration [13,14]. Two dependent variables that have been investigated recently are the intracellular steady-state concentration of H_2O_2 and the so-called latency (which describes the reduced average reaction rates for the observed decomposition of H_2O_2 due to the localization of encapsulated catalase in the peroxisomes). In [13], a lumped-parameter mathematical model, assuming that catalase is the major H_2O_2-removal enzyme, was developed and used to calculate the intracellular steady-state H_2O_2 concentration for several cell lines. The model was calibrated to the experimental values of the measured critical parameters, and the resulting intracellular steady-state H_2O_2 concentration was related to observed cell specific susceptibility to extracellular exposure of H_2O_2. The results showed that despite the fact that the experimental parameters including catalase concentration and H_2O_2 membrane diffusion rate constant, in particular, varied significantly across cell lines, the calculated steady-state intracellular-to-extracellular $[H_2O_2]$ ratio did not vary significantly across cell lines. In [14], it was investigated whether variations in the latency of peroxisomal catalase across cancer cell lines correlates with observed in vitro susceptibility to ascorbate at equivalent dosing of extracellular H_2O_2. The so-called effectiveness factor, which takes both the membrane diffusion rate and the overall reduced activity for encapsulated catalase into account, was used to quantify the effect of latency. The results suggest that latency alone is not a reliable parameter for predicting cell susceptibility to ascorbate (and hence, H_2O_2).

In this study, we explore new dependent variables that could possibly explain the difference in cell susceptibility to an external addition of H_2O_2, with and without a simultaneous addition of NO_2^-, and ultimately, quantify the effect in terms of the H_2O_2 membrane diffusion rate constant ($k_{D,1}$) and the intracellular catalase concentration ($[CATFe^{III}]_0$). Since we cannot distinguish a cancer cell from a normal cell solely by their H_2O_2 membrane diffusion rate constant and intracellular catalase concentration, we will have to work under the notations "cancer-like cells" (i.e., systems in the higher range of H_2O_2 membrane diffusion rate constant and the lower range of catalase concentration) and "normal-like cells" (i.e., systems in the lower range of H_2O_2 membrane diffusion rate constant and the higher range of catalase concentration). We investigate different regimes of the supplied extracellular H_2O_2- and NO_2^- concentrations according to experimental observations of the regimes of selective/non-selective and synergistic/non-synergistic anti-cancer effect of PTL [25,26]. The dependent variables that we investigate are:

1. **The temporal maximum of $[H_2O_2]$ and $[ONOO^-]$ in the IC.** As opposed to the steady-state value of the intracellular H_2O_2 concentration, the temporal maximum can be expected to be dependent on both $k_{D,1}$ and $[CATFe^{III}]_0$. These dependent variables may be related to the maximal intracellular oxidative power of the extracellularly added H_2O_2 (and NO_2^-), and thus it would be of interest to study whether a certain extracellularly added concentration of H_2O_2 (and NO_2^-) would result in a higher oxidative power in a more cancer-like cell than in a more normal-like cell.
2. **The system response time (i.e., the time out of equilibrium) with respect to $[H_2O_2]$ in the IC.** In order to achieve tumor progression, it is essential for cancer cells to optimize their RONS concentration and maintain the RONS equilibrium. For our mathematical model, this is translated into the question: does a more cancer-like cell have a longer response time compared to a more normal-like cell?
3. **The "load" of intracellular H_2O_2 and $ONOO^-$ (i.e., the time integral of $[H_2O_2]$ and $[ONOO^-]$ in the IC).** As the temporal maximum of $[H_2O_2]$ and $[ONOO^-]$ cannot capture any information about the total "load" of H_2O_2 and $ONOO^-$ (i.e., how much the intracellular $[H_2O_2]$ and $[ONOO^-]$ is increased over a period of time), it could be of interest to study such a dependent variable as a complement. The load can be seen as a measure that combines the temporal maximum concentration and the system

response time. Another possible way to define the load of intracellular H_2O_2 would be to only consider the concentration of H_2O_2 over a "baseline". Here, the steady-state intracellular $[H_2O_2]$, before the perturbation of an addition of extracellular H_2O_2 and at the upper limit of $[CATFe^{III}]_0$, is used as the baseline.

4. **The inverse of the average and maximal rate of extracellular H_2O_2 consumption.** Since the cell susceptibility of CAP and PTL has been found to be inversely proportional to the (extracellular) consumption rate of H_2O_2, it is of interest to explore a dependent variable quantifying the system susceptibility in terms of the H_2O_2 consumption. We investigate two such candidates where one was defined in terms of the inverse of the average H_2O_2 consumption rate, and the other one in terms of the inverse of the maximal H_2O_2 consumption rate.

For all proposed dependent variables, we will analyze the dependence on $k_{D,1}$ and $[CATFe^{III}]_0$ and whether a more cancer-like cell is associated with a higher "response" than a more normal-like cell. Our main research question is thus: Can the difference in cell susceptibility toward PTL be understood, and even quantified, by one of these dependent variables?

To the best of our knowledge, this is the first study of its kind, and our aim is to take some initial steps in the direction of an increased understanding of the mechanisms underlying the selective and synergistic anti-cancer effect of PTL, and ultimately, be able to predict the response of different cells.

3. Results

As introduced in Section 2.2, in order to try to understand the combined role of the H_2O_2 membrane diffusion rate constant and the intracellular catalase concentration in determining the susceptibility of cells toward exogenous H_2O_2, we have to go beyond the steady-state value of the intracellular H_2O_2 concentration [13] (as well as latency [14]) and examine dependent variables that take the system's temporal response of a $[H_2O_2]$ perturbation in the EC into account. To be able to present the results in a more compact manner, the variables not yet introduced but of importance, and their denotations, are presented in Table 1. Details about the independent and dependent variables can be found in Section 5, where the mathematical model is presented. Likewise, details about the numerical calculations such as the values of the independent variables and parameters used in the model, can be found in Section 6.

Table 1. Denotations of variables used in the results analysis.

Variable	Meaning
$[H_2O_2]_0^{EC}$	Initial $[H_2O_2]$ in the EC
$[NO_2^-]_0^{EC}$	Initial $[NO_2^-]$ in the EC
$[H_2O_2]^{IC}$	$[H_2O_2]$ in the IC
$c_{1,\max}$	Temporal maximum of $[H_2O_2]$ in the IC

For the analysis and interpretation of the results, we mainly consider three important features of the dependent variable of interest:

- Does it account for selectivity with respect to different regimes of $[H_2O_2]_0^{EC}$?
- Does it account for a synergistic effect when NO_2^- is added to the system?
- Does it represent a feasible measure to quantify the susceptibility to exogenous H_2O_2 of a cell system in terms of $k_{D,1}$ and $[CATFe^{III}]_0$?

To qualify as a "measure" (i.e., as a quantification of the susceptibility in terms of $k_{D,1}$ and $[CATFe^{III}]_0$), the dependent variable should be associated with a higher value for cells with a higher susceptibility and a lower value for cells with a lower susceptibility. Thus, in accordance with experimental observations, a feasible measure should result in a higher value for more cancer-like cells than for more normal-like cells, at least in the expected

regime of selectivity (that is, for $[H_2O_2]_0^{EC}$ in the μM-range [26]). However, it should be noted that in this study, we do not follow strict mathematical criteria for a function to be categorized as a measure.

3.1. The Temporal Maximum of the Intracellular Hydrogen Peroxide Concentration: A Possible Measure of the Cell Susceptibility to Exogenous Hydrogen Peroxide

Our calculation results suggest that the temporal maximum of $[H_2O_2]^{IC}$ (i.e., $c_{1,\max}$) is the dependent variable of major interest in terms of our requirements. Therefore, we focus our analysis on this variable. The results of the other dependent variables are presented in Appendix A.

Figure 2 shows $c_{1,\max}$ as a function of $k_{D,1}$ and $[CATFe^{III}]_0$ for $[H_2O_2]_0^{EC} = 1$ μM, with and without NO_2^-. The same results, but for $[H_2O_2]_0^{EC} = 1$ mM, are shown in Figure 3.

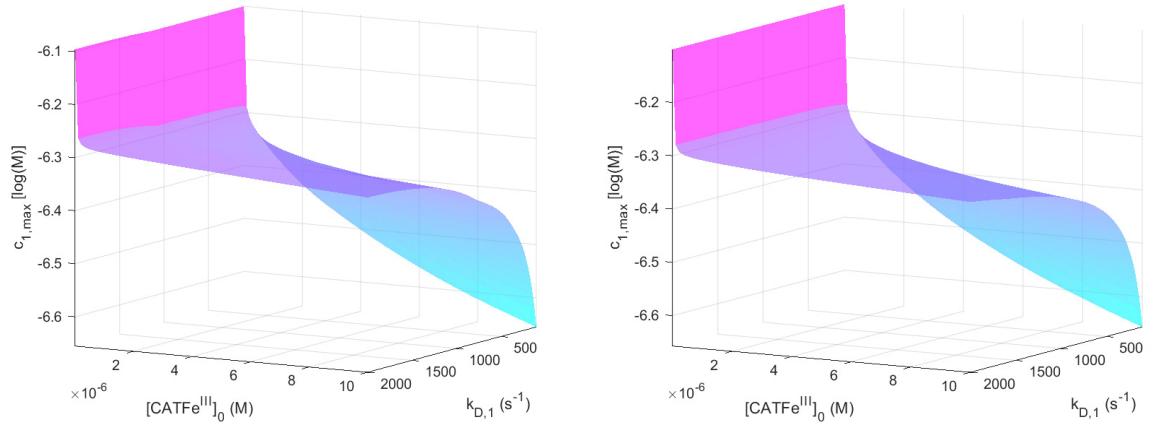

Figure 2. The dependent variable $c_{1,\max}$ (i.e., the temporal maximum of $[H_2O_2]$ in the IC) as a function of $k_{D,1}$ and $[CATFe^{III}]_0$ when $[H_2O_2]_0^{EC} = 1$ μM. $[NO_2^-]_0^{EC} = 0$ M (**a**) and $[NO_2^-]_0^{EC} = 1$ mM (**b**).

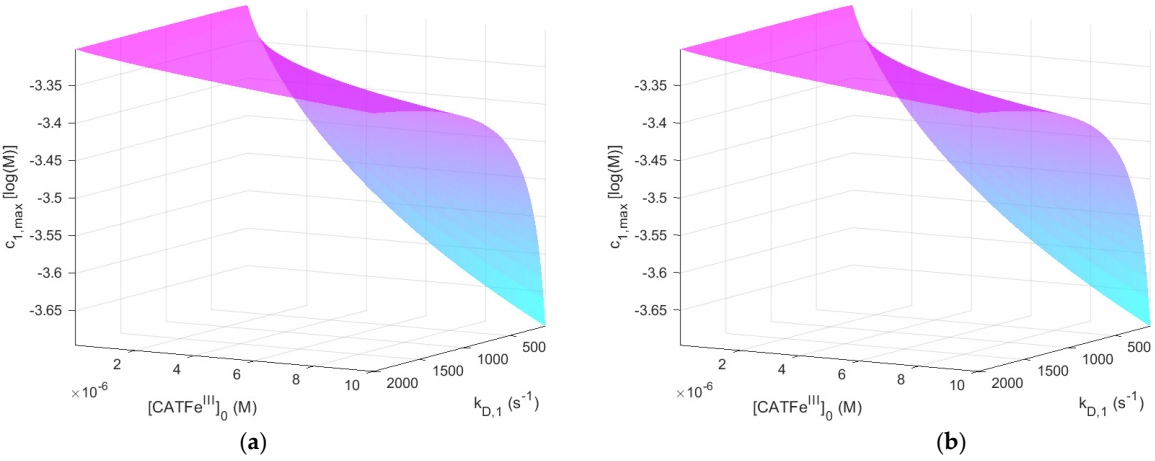

Figure 3. The dependent variable $c_{1,\max}$ (i.e., the temporal maximum of $[H_2O_2]$ in the IC) as a function of $k_{D,1}$ and $[CATFe^{III}]_0$ when $[H_2O_2]_0^{EC} = 1$ mM. $[NO_2^-]_0^{EC} = 0$ M (**a**) and $[NO_2^-]_0^{EC} = 1$ mM (**b**).

When comparing the result for the different $[H_2O_2]_0^{EC}$-regimes for $[NO_2^-]_0^{EC} = 0$ M (see Figures 2a and 3a), we see that $c_{1,\max}$ is also in different concentration regimes, which is logical. Indeed, for $[H_2O_2]_0^{EC} = 1$ mM, $c_{1,\max} \gtrsim 10^{-4}$ M, whereas for $[H_2O_2]_0^{EC} = 1$ μM, $c_{1,\max} < 10^{-6}$ M. Thus, by assuming that there exists a threshold value $c_{1,\max} > 10^{-6}$ M for which all types of cells undergo cell death, selectivity could be accounted for. However, there is no obvious synergetic effect; when comparing Figure 2a,b, $c_{1,\max}$ is almost identical.

Thus, the addition of NO_2^- does not change $c_{1,\max}$ significantly. The same is true for Figure 3a,b.

For $[H_2O_2]_0^{EC} = 1$ µM, $c_{1,\max}$ shows an increased $k_{D,1}$-dependence with increasing $[CATFe^{III}]_0$. The lowest value of $c_{1,\max}$ is for the lowest values of $k_{D,1}$ and highest values of $[CATFe^{III}]_0$, as would be expected for a dependent variable that would qualify as a measure of the cell susceptibility in terms of $k_{D,1}$ and $[CATFe^{III}]_0$. In addition, the highest value of $c_{1,\max}$ is associated with the lowest value of $[CATFe^{III}]_0$. However, in this regime, the dependence on $k_{D,1}$ is insignificant. Here, in contrast, there exists a significant $[CATFe^{III}]_0$-dependence and by changing the scale on the $[CATFe^{III}]_0$-axis to a log-scale (see Figure 4), we see that there are two distinct regimes with a clear shift from one regime to another at about $[CATFe^{III}]_0 \sim 10^{-7}$ M. The regimes of $k_{D,1}$ and $[CATFe^{III}]_0$ with the most profound difference between the value of $c_{1,\max}$ is between cells with $[CATFe^{III}]_0 < 10^{-7}$ M (for all $k_{D,1}$) and cells with the lowest possible $k_{D,1}$ and highest possible $[CATFe^{III}]_0$. Thus, $c_{1,\max}$ (i.e., the temporal maximum of $[H_2O_2]^{IC}$) is associated with a higher value for cancer-like cells than for normal-like cells. Indeed, $c_{1,\max}$ is about four times greater for the most susceptible cells compared to the most resistant cells.

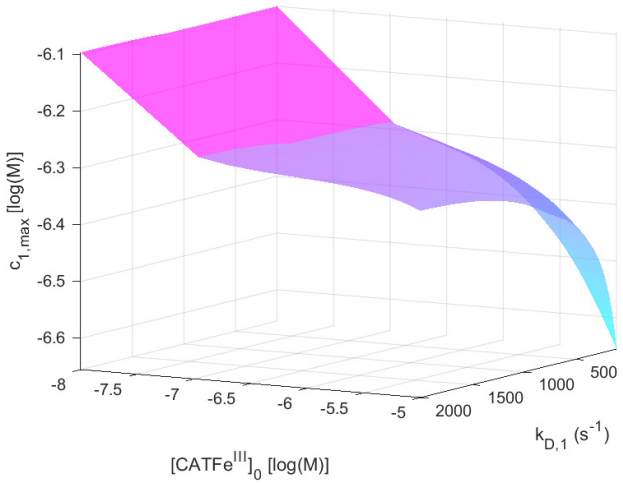

Figure 4. The dependent variable $c_{1,\max}$ (i.e., the temporal maximum of $[H_2O_2]$ in the IC) as a function of $k_{D,1}$ and $\log([CATFe^{III}]_0)$ when $[H_2O_2]_0^{EC} = 1$ µM and $[NO_2^-]_0^{EC} = 0$ M.

In summary, $c_{1,\max}$ does capture the dependence of $k_{D,1}$ and $[CATFe^{III}]_0$ in a manner that is consistent with experimental observations and could thus represent a feasible measure to quantify the susceptibility of different cells in terms of their H_2O_2 membrane diffusion rate constant and intracellular catalase concentration. However, in our model, it cannot yet account for the synergistic effect when NO_2^- is added.

To the best of our knowledge, there are not yet any experimental results to support our findings. We hope that our theoretical work will inspire future experimental studies. In the next section (Section 3.2), we discuss possible opportunities to experimentally quantify $c_{1,\max}$.

3.2. Physical Interpretation and the Use of the Temporal Maximum of the Intracellular Hydrogen Peroxide Concentration as an Experimental Probe

Our model, with all the equations, is explained in detail in Section 5. Here we use the equations to better understand how we can use $c_{1,\max}$ as a measure to quantify the response of different cells. In order to analyze and write the equations in a more compact manner, we first introduce some short notations as well as some new notations (see Table 2).

Table 2. Denotations of variables used in the results analysis.

Variable	Meaning
c_1^{IC}	$[H_2O_2]^{IC}$
c_1^{EC}	$[H_2O_2]^{EC}$
c_2	$\left[CATFe^{III}\right]$
c_3	$\left[CATFe^{IV}O^{\bullet+}\right]$
k_P	Rate of mitochondrial H_2O_2 production
k_1	Rate of H_2O_2 consumption by $\left[CATFe^{III}\right]$
k_2	Rate of H_2O_2 consumption by $\left[CATFe^{IV}O^{\bullet+}\right]$

The temporal maximum of c_1^{IC} (i.e., $c_{1,\max}$) occurs when the production and consumption of intracellular H_2O_2 are equal and $c_1^{EC} - c_1^{IC} \geq 0$ (as opposed to the steady-state value of $[H_2O_2]^{IC}$, which is governed by the same rate equation but for which $c_1^{EC} - c_1^{IC} = 0$). If we exclude in Equation (10) (see Section 5.2.2) the term representing the formation of $ONOOH$ from H_2O_2 and NO_2^- (since it is much smaller than the other terms), we have

$$-k_1 c_{1,\max} c_2 - k_2 c_{1,\max} c_3 + k_{D,1}\left(c_1^{EC} - c_{1,\max}\right) + k_P = 0.$$

Thus,

$$k_{D,1}\left(c_1^{EC} - c_{1,\max}\right) + k_P = k_1 c_{1,\max} c_2 + k c_{1,\max} c_3.$$

Here, we can furthermore use the constraint

$$c_3 = \left[CATFe^{III}\right]_0 - \left[CATFe^{III}\right],$$

since the total catalase concentration will be constant. By noting that $k_1 \sim k_2 = k$ (see Section 6.2.1), we can use the approximate expression

$$k_{D,1}\left(c_1^{EC} - c_{1,\max}\right) + k_P = k c_{1,\max}\left[CATFe^{III}\right]_0.$$

From our numerical calculations, we know that for low $\left[CATFe^{III}\right]_0$, $c_{1,\max}$ is independent on $k_{D,1}$, whereas for high $\left[CATFe^{III}\right]_0$, $c_{1,\max}$ is highly dependent on $k_{D,1}$. Furthermore (for $\left[CATFe^{III}\right]_0 > 10^{-7}$ M), for low $k_{D,1}$, $c_{1,\max}$ is highly dependent on $\left[CATFe^{III}\right]_0$, whereas for high $k_{D,1}$, $c_{1,\max}$ is independent on $\left[CATFe^{III}\right]_0$. The question is whether this behavior can be understood.

In the analysis, we first note that the implicit importance of $\left[CATFe^{III}\right]_0$ and $k_{D,1}$ in determining the value of c_1^{EC} at the time of $c_{1,\max}$, and thus $c_{1,\max}$, is hidden. The dependence on $\left[CATFe^{III}\right]_0$ originates from the fact that in our model, $c_{1,0}^{IC}$ is determined by $\left[CATFe^{III}\right]_0$. Equation (3) (in Section 5.2.1) can be approximated as:

$$\frac{dc_1^{EC}}{dt} = -k_{D,1}\left(c_1^{EC} - c_1^{IC}\right).$$

Hence, the initial rate, or driving force, of H_2O_2-consumption in the EC will crucially depend on $c_{1,0}^{IC}$, and thus, $\left[CATFe^{III}\right]_0$. In fact, $c_{1,0}^{IC} \sim 10^{-7}$ M for $\left[CATFe^{III}\right]_0 \sim 10^{-8}$ M, whereas $c_{1,0}^{IC} \sim 10^{-10}$ M for $\left[CATFe^{III}\right]_0 \sim 10^{-5}$ M (see Equation (18), Section 6). It means that the initial driving force is about ten times higher in the latter case compared to the former. This could explain why $c_{1,\max}$ is seemingly independent on $k_{D,1}$ at low values of $\left[CATFe^{III}\right]_0$; if $k_{D,1}\left(c_1^{EC} - c_{1,\max}\right) \ll k_P$ for all values of $k_{D,1}$, k_P will be the dominant factor of the build up of H_2O_2 in the IC. For higher values of $\left[CATFe^{III}\right]_0$, it seems like somewhen at $\left[CATFe^{III}\right]_0 > 10^{-7}$ M, $c_{1,\max}$ becomes increasingly dependent on $k_{D,1}$. It is thus reasonable to believe that the term $k_{D,1}\left(c_1^{EC} - c_{1,\max}\right)$ is becoming increasingly

dominant and that the larger the value of $\left[CATFe^{III}\right]_0$, the larger the value of $\left(c_1^{EC} - c_{1,\max}\right)$. For a fixed value of $\left[CATFe^{III}\right]_0$, $c_{1,\max}$ will thus increase with increasing values of $k_{D,1}$.

In summary, this means that the lower the value of $\left[CATFe^{III}\right]_0$, the less important is the value of $k_{D,1}$, and the other way around. Thus, the susceptibility (toward exogenous H_2O_2) of cancer-like cells is not much influenced by the H_2O_2 membrane diffusion rate constant and this is due to their much higher level of intracellular H_2O_2 prior to the perturbation by the addition of exogenous H_2O_2. Normal-like cells, on the other hand, are more sensitive to the value of the H_2O_2 membrane diffusion rate constant, since the difference in concentration between the intracellular and extracellular H_2O_2 will be much larger.

Another aspect of $c_{1,\max}$ is whether it could provide an opportunity to extract information about different cell lines in terms of their H_2O_2 membrane diffusion rate constant and intracellular catalase concentration. By measuring $c_{1,\max}$ and the corresponding c_1^{EC} for different $c_{1,0}^{EC}$ it could be possible to roughly quantify $k_{D,1}$ and $\left[CATFe^{III}\right]_0$. There are many experimental techniques for the detection and quantification of the H_2O_2 concentration in vitro and in vivo. The intracellular H_2O_2 concentration has been detected and measured by a chemoselective fluorescent naphthylimide peroxide probe [70], by a genetically encoded red fluorescent sensor [71], and by fluorescent reporter proteins [72]. Thus, even if $c_{1,\max}$ does not represent a feasible measure of the cell susceptibility in terms of $k_{D,1}$ and $\left[CATFe^{III}\right]_0$, it could still possibly be used to gain more knowledge about the correlation between $k_{D,1}$ and $\left[CATFe^{III}\right]_0$ and cell susceptibility toward exogenous H_2O_2 and PTLs.

4. Discussion

In this study, we use a theoretical approach to increase the knowledge about possible underlying causes of the anti-cancer effect of PTL. Although the model is fairly simple, it does include the major pathways for species production and consumption relevant for such a cell system. It also puts emphasis on two important features (i.e., the H_2O_2 membrane diffusion rate constant and the intracellular catalase concentration), possibly explaining the different cell responses and cell susceptibility toward PTL when comparing normal cells to cancer cells, but also when comparing resistant vs. sensitive cancer cells. Nevertheless, it is important to keep in mind that in our model, different cells are only defined in terms of these two features, which are independent variables in our analysis, whereas in reality, there are countless of other features characteristic for different types of cells that could play an important role in the context of the anti-cancer effect of PTL. Here, we merely analyze the immediate cell response determined by the scavenging system active at high concentrations of H_2O_2. However, we do believe that our results contribute to a better understanding of some mechanisms probably underlying the anti-cancer effect of PTL. It brings novelty to the field of plasma oncology, and more broadly to the field of redox biology by using a theoretical approach and by proposing new ways to quantify the selective and synergistic anti-cancer effect of PTL in terms of inherent factors of cells. Here, we discuss each of our main findings and their potential implications. We also highlight what we believe are the most important limitations of the model.

As opposed to the steady-state intracellular concentration of H_2O_2, which has been evaluated in previous studies [13], our results suggest that the temporal maximal concentration of intracellular H_2O_2 could be a measure feasible to quantify the cell susceptibility toward exogenous H_2O_2 in terms of the H_2O_2 membrane diffusion rate constant and the intracellular catalase concentration. This result furthermore enables us to speculate whether the mode of action of H_2O_2 is as a signaling molecule rather than as a toxic substance causing necrosis. It is known that the intracellular concentration of a signaling molecule rises and falls within a short period. Indeed, whether a signaling molecule is effective or not is determined by how rapidly it is produced, how rapidly it is removed, and the concentration it must reach to alter the activity of its target effector. Of particular relevance in our context is that several reports have demonstrated that the rate of H_2O_2 generation and its concentration as a function of time play a key role in determining target cell damage

or destruction [73–75]. RONS are regulators of signaling pathways such as the extracellular signal-regulated kinase (ERK) mitogen activated protein kinase (MAPK) pathway, which is important for cell proliferation, and a number of studies have demonstrated the ability of exogenous oxidants to activate the ERK MAPK pathway [76–80]. As in the general case, the duration and intensity of the ERK MAPK signal determine the outcome of the cellular response; there is a connection between the levels of ROS in a cell and the levels of MAPK signaling. In particular, MAPKs are activated in response to H_2O_2 [81–83].

Based on our modeling results (presented in the Appendix A; i.e., Figures A1 and A9), we do not think that the formation of $ONOO^-$ itself plays a major role in the explanation of the synergistic effect of H_2O_2 and NO_2^-. This is because although the overall intracellular concentration of $ONOO^-$ is increased with about one order of magnitude when NO_2^- is added to the system, the dependence on the H_2O_2 membrane diffusion rate constant is such that cells with a higher value of the H_2O_2 membrane diffusion rate constant (i.e., cancer-like cells) are associated with a lower maximal intracellular $ONOO^-$ concentration than more normal-like cells (i.e., cells with a lower value of the H_2O_2 membrane diffusion rate constant). In addition, the load of $ONOO^-$ is independent of the H_2O_2 membrane diffusion rate constant. However, an important aspect to keep in mind regarding our results for $ONOO^-$ and the choice to include CO_2-catalyzed consumption of $ONOO^-$ in our model, is that CO_2 redirects much of the $ONOO^-$ produced in vivo toward radical mechanisms [65]. Indeed, many of the reactions of $ONOO^-$ in vivo are more likely to be mediated by reactive intermediates derived from the reaction of $ONOO^-$ with CO_2 than by $ONOO^-$ itself [84,85]. Thus, if the production of such reactive intermediates were to be monitored instead of $ONOO^-$, our results might be different. In this context, especially the formation of $CO_3^{\bullet -}$ should be considered; a fraction (about 30%) of the formed $ONOOCOO^-$ will produce cage-escaped $^\bullet NO_2$ and $CO_3^{\bullet -}$ radicals according to [86–88]

$$ONOOCOO^- \rightleftharpoons CO_3^{\bullet -} + {}^\bullet NO_2,$$

where $k = 1.9 \times 10^9$ s^{-1} and $k' = 5 \times 10^8$ $M^{-1}s^{-1}$ [89]. A possibly important target in the context of our study is catalase; catalase is so far the best known protein target for $CO_3^{\bullet -}$ and the rate constant of the reaction of bovine liver catalase with $CO_3^{\bullet -}$ is $(3.7 \pm 0.4) \times 10^9$ $M^{-1}s^{-1}$ at $pH = 8.4$ [90]. Since the temporal maximum of intracellular $[H_2O_2]$ (i.e., $c_{1,\max}$) is inversely dependent on the catalase concentration (i.e., $[CATFe^{III}]_0$) with an increasingly steeper incline for lower catalase concentrations in the regime $10^{-8} \leq [CATFe^{III}]_0 \leq 10^{-7}$ M (see Figure 2), cancer-like cells would be more vulnerable to a decrease in the catalase concentration than normal-like cells, which are associated with higher values of $[CATFe^{III}]_0$. Thus, including these reaction pathways may possibly also make the dependent variable $c_{1,\max}$ able to account for the synergetic effect of NO_2^-. Such an extension of our model was out of the scope for this study, but would be highly interesting in a future model development.

In experiments, the consumption rate of extracellular H_2O_2 has been found to inversely correlate with the susceptibility of cancer cells toward exogenous H_2O_2 [32]. Thus, cancer cell lines with a high consumption rate were less susceptible. Our results cannot yet account for this correlation; when cells are defined in terms of their H_2O_2 membrane diffusion rate constant and their intracellular catalase concentration, susceptibility in terms of the inverse of the extracellular H_2O_2 consumption rate is not consistent with the experimental observations of cancer cells having a higher H_2O_2 membrane diffusion rate constant and a lower catalase concentration (see Section 2.1). The fact that our model does not reproduce these patterns leaves an open question of how to construct a dependent variable in terms of the inverse of the extracellular H_2O_2 consumption rate so that it corresponds to the experimental correlation.

The fact that our mathematical model, as well as our criteria for a dependent variable to represent a feasible measure of the cell susceptibility, does not select the system response time as a good candidate does not necessarily indicate that this variable, in general, cannot capture cell susceptibility toward exogenous H_2O_2. Indeed, in our definition of this depen-

dent variable, we assume a tolerance of a 10% increase of the intracellular steady-state H_2O_2 concentration, and a different assumption of the tolerance might give a different result.

Except for the limitations of the model already mentioned in this discussion, some other model assumptions could hamper a realistic representation of a cell system in interaction with PTL. One such limitation is that in our model, the rate of mitochondrial H_2O_2 production is constant. Although it can be argued that this assumption is a valid starting point, in a model development, it could be important to modify this aspect to represent a cancer cell in a more realistic manner. Indeed, it has been shown that in some cancer cells, the mitochondrial respiration is decreased (in favor of aerobic glycolysis), and moreover, this shift seems to be a dynamic process (see [91] and references therein). We believe that future models could benefit from trying to take such variation of the rate of mitochondrial H_2O_2 production into account, but this was out of the scope for this study.

Another aspect to take into account in a more realistic model is the fact that the H_2O_2 membrane diffusion rate constant is not a static but dynamic property. In [92], it was shown that cellular stress conditions reversibly inhibit the diffusion of H_2O_2 (and H_2O) of aquaporin 8. Thus, a more complex model taking the implicit time-dependence of the H_2O_2 membrane diffusion rate (caused by the increased intracellular H_2O_2 concentration after the addition of exogenous H_2O_2) could potentially produce results different from our model.

A third aspect to be aware of is that in our model, we assume that the addition of PTL does not affect the membrane diffusion rate constants. However, a number of studies have reported an enhanced cell membrane permeability (and thus, increased membrane diffusion rate constants) after CAP/PTL treatment [93–95]. For the aim and approach of our study, where the membrane diffusion rate constant of the key species H_2O_2 is varied within a range of possible values, we believe that our assumption is a valid starting point. Nevertheless, for future model extensions and developments, this aspect might be important to take into account.

Finally, it should be mentioned that the rate equations used to model the system are derived from information (collected from the literature) about rate constants and reaction orders for each reaction as they appear in the experiments. Most likely, the experimental conditions will deviate from the conditions of cells treated with PTL, which will affect the accuracy of the results produced by the model. However, for the purpose of our study, we believe that parameter values of the correct order of magnitude are sufficient at this stage.

5. Mathematical Model

Mathematical models of biological reaction networks such as the system considered in this study, can generally be divided into two categories: predictive and descriptive models. Since the experimental studies on which we build our model on are primarily in vitro studies, we construct a predictive model in this work. This means that we put together the information about each of the involved reactions (reaction orders, rate constants, etc.) as they appear in the experiments. From there, the result for a certain set of initial conditions is generated by solving the time-dependent equations of motion, representing the time evolution of the system.

In this section, we systematically present the species and reactions in the system considered (Section 5.1), how the system time evolution is modeled (Section 5.2), and we explicitly define the dependent variables that are analyzed (Section 5.3).

5.1. Species and Reactions in the System

The involved species of interest are H_2O_2, NOO^-, $ONOOH$, NO_2^-, CO_2, H^+, $CATFe^{III}$ and $CATFe^{IV}O^{\bullet+}$ (see Figure 1 in Section 2). The following reactions and interactions of the species H_2O_2, NO_2^- and (native) catalase $\left(CATFe^{III}\right)$ in the system are taken into account.

- Decomposition of H_2O_2 by catalase:

$$CATFe^{III} + H_2O_2 \xrightarrow{k_1} CATFe^{IV}O^{\bullet+} + H_2O,$$

$$CATFe^{IV}O^{\bullet+} + H_2O_2 \xrightarrow{k_2} CATFe^{III} + O_2 + H_2O.$$

- Generation of $ONOO^-$ through reaction between H_2O_2 and NO_2^-:

$$NO_2^- + H_2O_2 + H^+ \xrightarrow{k_3} ONOOH + H_2O,$$

where the equilibrium between $ONOOH$ and $ONOO^-$ is described by:

$$ONOOH \underset{k_{-4}}{\overset{k_4}{\rightleftharpoons}} ONOO^- + H^+.$$

- Decomposition of $ONOO^-$ by catalase:

$$2ONOO^- \xrightarrow[CATFe^{III}]{k_5} O_2 + 2NO_2^-.$$

- CO_2-catalyzed consumption of $ONOO^-$:

$$ONOO^- + CO_2 \xrightarrow{k_6} ONOOCOO^-.$$

The denotations of the time-dependent concentrations of the different species are shown in Table 3.

Table 3. Denotations of the time-dependent concentrations in the system.

Species	Denotation
$[H_2O_2]$	c_1
$[CATFe^{III}]$	c_2
$[CATFe^{IV}O^{\bullet+}]$	c_3
$[ONOO^-]$	c_4
$[NO_2^-]$	c_5
$[H^+]$	c_6
$[ONOOH]$	c_7
$[CO_2]$	c_8

5.2. Modeling the System

The mathematical model considers the kinetics of the reactions in the system composed of two subsystems (EC and IC), see Figure 1 in Section 2, as well as diffusion of certain species between the two subsystems. The equation governing the kinetics of each species i is given by the sum of the reaction rates (describing the rate of production and consumption of species i),

$$\frac{dc_i}{dt} = r_i, \tag{1}$$

and (in the case of species 1, 4, 5, and 7), the diffusion rate through the cell membrane, from the EC to the IC,

$$\frac{dc_i}{dt} = -k_{D,i}\left(c_i^{EC} - c_i^{IC}\right). \tag{2}$$

Equation (1) represents the resulting rate equation, derived from the rate constants and reaction orders for each reaction as they appear in the experiments. Equation (2)

describes the rate of membrane diffusion of species i according to Fick's law of diffusion with a linear concentration gradient over the cell membrane. Here, $k_{D,i}$ is the rate of species i exchange through the membrane. We denote this as "membrane diffusion rate constant". More information about the derivation of Equation (2) can be found in Appendix B.

Explicitly, our mathematical model is used to analyze the behavior of a dependent variable $y(\overline{x})$, where $\overline{x}$ denotes the set of independent variables that are varied in the system. The independent variables in our model are:

- The H_2O_2 membrane diffusion rate constant through the cell membrane ($k_{D,1}$) and
- The initial intracellular catalase concentration ($[CATFe^{III}]_0$).

The species CO_2 and H^+ are assumed to be present in equal initial concentrations in both the EC and the IC (thus, $c_{8,0}^{EC} = c_{8,0}^{IC}$ and $c_{6,0}^{EC} = c_{6,0}^{IC}$). Since we do not explicitly study the kinetics of these species, we make such an assumption to reduce the complexity of the model.

Detailed information about the mathematical model is presented in the following sections.

5.2.1. Mathematical Model of the Reaction Kinetics in the Extracellular Compartment

At $t = 0$, H_2O_2 and NO_2^- in certain initial concentrations ($c_{1,0}^{EC} = [H_2O_2]_0^{EC}$ and $c_{5,0}^{EC} = [NO_2^-]_0^{EC}$) are inserted into the EC, representing treatment of the cell by PTL (as these species are the dominant RONS in PTLs), and their reactions as well as diffusion through the membrane into the IC is monitored. The reaction network and resulting set of differential equations are given below.

- Reaction network

$$NO_2^- + H_2O_2 + H^+ \overset{k_3}{\rightarrow} ONOOH + H_2O,$$

$$ONOOH \underset{k_{-4}}{\overset{k_4}{\rightleftharpoons}} ONOO^- + H^+,$$

$$ONOO^- + CO_2 \overset{k_6}{\rightarrow} ONOOCOO^-,$$

$$H_2O_2 \overset{k_{D,1}}{\rightarrow} IC,$$

$$ONOO^- \overset{k_{D,4}}{\rightarrow} IC,$$

$$NO_2^- \overset{k_{D,5}}{\rightarrow} IC,$$

$$ONOOH \overset{k_{D,7}}{\rightarrow} IC.$$

- Differential equations

$$\frac{dc_1^{EC}}{dt} = -k_3 c_1^{EC} c_5^{EC} c_6^{EC} - k_{D,1}\left(c_1^{EC} - c_1^{IC}\right), \quad (3)$$

$$\frac{dc_4^{EC}}{dt} = k_4 c_7^{EC} - k_{-4} c_4^{EC} c_6^{EC} - k_6 c_4^{EC} c_8^{EC} - k_{D,4}\left(c_4^{EC} - c_4^{IC}\right), \quad (4)$$

$$\frac{dc_5^{EC}}{dt} = -k_3 c_1^{EC} c_5^{EC} c_6^{EC} - k_{D,5}\left(c_5^{EC} - c_5^{IC}\right), \quad (5)$$

$$\frac{dc_6^{EC}}{dt} = -k_3 c_1^{EC} c_5^{EC} c_6^{EC} + k_4 c_7^{EC} - k_{-4} c_4^{EC} c_6^{EC}, \tag{6}$$

$$\frac{dc_7^{EC}}{dt} = k_3 c_1^{EC} c_5^{EC} c_6^{EC} - k_4 c_7^{EC} + k_{-4} c_4^{EC} c_6^{EC} - k_{D,7}\left(c_7^{EC} - c_7^{IC}\right), \tag{7}$$

$$\frac{dc_8^{EC}}{dt} = -k_6 c_4^{EC} c_8^{EC}. \tag{8}$$

5.2.2. Mathematical Model of the Reaction Kinetics in the Intracellular Compartment

At $t = 0$, the concentration of H_2O_2 is at a certain steady-state value ($c_{1,0}^{IC} = [H_2O_2]_0^{IC}$) because it is continuously produced by the mitochondria at the rate

$$\frac{dc_1^{IC}}{dt} = k_P, \tag{9}$$

and decomposed by catalase, which exists in the IC, and is modeled as free in the solution. (More information can be found in Section 6.2.3). It is assumed that at $t = 0$, the total amount of catalase exists as $CATFe^{III}$ (i.e., $c_{3,0}^{IC} = 0$). The reaction network and resulting set of differential equations are given below.

- Reaction network

$$CATFe^{III} + H_2O_2 \overset{k_1}{\rightarrow} CATFe^{IV}O^{\bullet+} + H_2O,$$

$$CATFe^{IV}O^{\bullet+} + H_2O_2 \overset{k_2}{\rightarrow} CATFe^{III} + O_2 + H_2O,$$

$$NO_2^- + H_2O_2 + H^+ \overset{k_3}{\rightarrow} ONOOH + H_2O,$$

$$ONOOH \underset{k_{-4}}{\overset{k_4}{\rightleftharpoons}} ONOO^- + H^+,$$

$$2ONOO^- \overset{k_5}{\rightarrow} O_2 + 2NO_2^-,$$

$$ONOO^- + CO_2 \overset{k_6}{\rightarrow} ONOOCOO^-,$$

$$EC \overset{k_{D,1}}{\rightarrow} H_2O_2,$$

$$EC \overset{k_{D,4}}{\rightarrow} ONOO^-,$$

$$EC \overset{k_{D,5}}{\rightarrow} NO_2^-,$$

$$EC \overset{k_{D,7}}{\rightarrow} ONOOH.$$

- Differential equations

$$\frac{dc_1^{IC}}{dt} = -k_1 c_1^{IC} c_2 - k_2 c_1^{IC} c_3 - k_3 c_1^{IC} c_5^{IC} c_6^{IC} + k_{D,1}\left(c_1^{EC} - c_1^{IC}\right) + k_P, \tag{10}$$

$$\frac{dc_2}{dt} = -k_1 c_1^{IC} c_2 + k_2 c_1^{IC} c_3, \tag{11}$$

$$\frac{dc_3}{dt} = k_1 c_1^{IC} c_2 - k_2 c_1^{IC} c_3, \tag{12}$$

$$\frac{dc_4^{IC}}{dt} = k_4 c_7^{IC} - k_{-4} c_4^{IC} c_6^{IC} - k_5 c_2 c_4^{IC} - k_6 c_4^{IC} c_8^{IC} + k_{D,4}\left(c_4^{EC} - c_4^{IC}\right), \tag{13}$$

$$\frac{dc_5^{IC}}{dt} = -k_3 c_1^{IC} c_5^{IC} c_6^{IC} + k_5 c_2 c_4^{IC} + k_{D,5}\left(c_5^{EC} - c_5^{IC}\right), \tag{14}$$

$$\frac{dc_6^{IC}}{dt} = -k_3 c_1^{IC} c_5^{IC} c_6^{IC} + k_4 c_7^{IC} - k_{-4} c_4^{IC} c_6^{IC}, \tag{15}$$

$$\frac{dc_7^{IC}}{dt} = k_3 c_1^{IC} c_5^{IC} c_6^{IC} - k_4 c_7^{IC} + k_{-4} c_4^{IC} c_6^{IC} + k_{D,7}\left(c_7^{EC} - c_7^{IC}\right), \tag{16}$$

$$\frac{dc_8}{dt}^{IC} = -k_6 c_4^{IC} c_8^{IC}. \tag{17}$$

Equations (3)–(8) and (10)–(17) are solved numerically. The details about the numerical calculations can be found in Section 6.3.

5.3. Dependent Variables

In the following sections, we explicitly define the dependent variables analyzed in this study.

5.3.1. Temporal Maximum of the Intracellular Hydrogen Peroxide and Peroxynitrite Concentration

The dependent variables $c_{1,\max}$ and $c_{4,\max}$ are defined as

$$c_{1,\max}\left(k_{D,1}, [CATFe^{III}]_0\right) = \max\left([H_2O_2]^{IC}\right),$$

and

$$c_{4,\max}\left(k_{D,1}, [CATFe^{III}]_0\right) = \max\left([ONOO^-]^{IC}\right).$$

5.3.2. System Response Time of Intracellular Hydrogen Peroxide

Assuming that the system has a tolerance of an increase of 10% of the baseline H_2O_2 concentration (see Section 3.2), the dependent variable τ can be formulated

$$\tau\left(k_{D,1}, [CATFe^{III}]_0\right) = t \ni \frac{(100+10)}{100} \times \left[H_2O_2\right]_t^{IC} = [H_2O_2]_0^{IC}.$$

5.3.3. Load of Intracellular Hydrogen Peroxide and Peroxynitrite

The simplest way of creating a quantitative measure of the "load" of intracellular H_2O_2 and $ONOO^-$ is to use the time-integral over the whole time regime ($0 \leq t \leq t_f$) as the dependent variable, in other words,

$$l_1\left(k_{D,1}, [CATFe^{III}]_0\right) = \int_0^{t_f} [H_2O_2]^{IC},$$

and

$$l_4\left(k_{D,1}, [CATFe^{III}]_0\right) = \int_0^{t_f} [ONOO^-]^{IC}.$$

For the "load" over the baseline concentration of intracellular H_2O_2, if we denote this baseline constant $[H_2O_2]_{BS}^{IC}$, the dependent variable is defined as

$$l_{1,BS}(k_{D,1}, \left[CATFe^{III}\right]_0) = \int_0^{t_f} \left([H_2O_2]^{IC} - [H_2O_2]^{IC}_{BS} \right).$$

5.3.4. Rate of Extracellular Hydrogen Peroxide Consumption

Here, we first define the dependent variable r as

$$r(k_{D,1}, \left[CATFe^{III}\right]_0) = \frac{d[H_2O_2]^{EC}}{dt}.$$

The average extracellular consumption rate of H_2O_2 is then defined as

$$\bar{r} = \frac{1}{t_f} \int_0^{t_f} r dt,$$

and the maximal extracellular consumption rate of H_2O_2 as

$$r_{\max} = \max(|r|).$$

In order to create a potential measure (i.e., a dependent variable where a more cancer-like cell is associated with a higher susceptibility), we use the variables

$$\bar{s} = \frac{1}{\bar{r}},$$

and

$$s_{\max} = \frac{1}{r_{\max}},$$

in our calculations.

6. Numerical Calculations

6.1. Independent Variables

The two independent variables in the system are $k_{D,1}$ and $c_{2,0} = [CATFe^{III}]_0$ (i.e., the diffusion rate constant of H_2O_2 through the cell membrane from the EC to the IC, and the initial catalase concentration in the IC). Furthermore, we use four different combinations of $c^{EC}_{1,0} = [H_2O_2]^{EC}_0$ and $c^{EC}_{5,0} = [NO_2^-]^{EC}_0$ in our calculations. The motivation and details of these variables are given in the following sections, and have also been introduced in Section 2.

6.1.1. Membrane Diffusion Rate Constant of Hydrogen Peroxide

In [96], the diffusion rate constant for H_2O crossing lipid bilayers was found to be 920 s^{-1}. Due to the chemical similarities between H_2O and H_2O_2, we use this value as a reference value for $k_{D,1}$ and we vary $k_{D,1}$ within the range $100 \leq k_{D,1} \leq 2000$ s^{-1}.

6.1.2. Initial Catalase Concentration in the Intracellular Compartment

The intracellular concentration of catalase is calculated from two different premises (see Appendix C). Considering the rough estimates in both approaches, it seems reasonable to use an effective catalase concentration in the range of 10^{-8}–10^{-5} M in our calculations. As a reference value, catalase concentration in human blood cells is about 2–3 µM [97,98].

6.1.3. Initial Hydrogen Peroxide and Peroxynitrite Concentration in the Extracellular Compartment

Several publications have shown that H_2O_2 and NO_2^- are formed at concentrations ranging from µM to mM in plasma-treated liquids (PTLs) [99–102]. In this study, we use the initial conditions for $[H_2O_2]^{EC}$ and $[NO_2^-]^{EC}$ shown in Table 4. The different regimes of

these four combinations are specified in the last column. We assume that the selectivity is related to the concentration of extracellular H_2O_2 (i.e., selective cancer killing only occurs at low H_2O_2 concentrations (order of 1 μM [26]), while higher H_2O_2 concentrations (e.g., order of 1 mM) kill both cancer and normal cells) [25]. Based on this assumption, we want to compare the dependent variables for the selective versus non-selective regime. For both regimes (selective versus non-selective), we furthermore want to investigate whether a synergistic effect can be found (i.e., if the values of the dependent variables are enhanced when H_2O_2 and NO_2^- are added together) [25,26].

Table 4. Initial concentrations of H_2O_2 and NO_2^- in the extracellular compartment.

$[H_2O_2]^{EC}(M)$	$[NO_2^-]^{EC}(M)$	Regime
10^{-3}	10^{-3}	Non-selective, synergistic
10^{-3}	0	Non-selective, non-synergistic
10^{-6}	10^{-3}	Selective, synergistic
10^{-6}	0	Selective, non-synergistic

6.2. Parameter Values

6.2.1. Reaction Rate Constants

The used rate constants are summarized in Table 5, along with the references where the data is adopted from, and some remarks about the conditions for which these values were reported.

Table 5. Reaction rate constants.

Rate Constant	Parameter Value	Reference	Remark
k_1	1.7×10^7 $M^{-1}s^{-1}$	[103]	Mammalian catalases
k_2	2.6×10^7 $M^{-1}s^{-1}$	[103]	Mammalian catalases
k_3	1.1×10^3 $M^{-2}s^{-1}$	[37]	At $pH = 3.3$ and $T = 25$ °C
k_4	$K_a k_{-4} = 10^{-pK_a} k_{-4}$	[104,105]	The pK_a-value at $T = 25$ °C is 6.5–6.8
k_{-4}	$\sim 10^{10}$ $M^{-1}s^{-1}$	[106]	
k_5	1.7×10^6 $M^{-1}s^{-1}$	[64]	At $pH = 7.1$ and $T = 25$ °C
k_6	5.8×10^4 $M^{-1}s^{-1}$	[84]	At $T = 37$ °C, pH-independent

6.2.2. Membrane Diffusion Rate Constants

NO_2^-, when protonated (i.e., as HNO_2), is reported to diffuse easily across biological membranes [107]. When not protonated, anionic channels have been shown to be permeable to NO_2^- [108]. It has furthermore been established that $ONOO^-$ is able to penetrate cell membranes [96,109]. In [96], using model phospholipid vesicular systems, it was demonstrated that $ONOO^-$ freely crosses phospholipid membranes. The diffusion rate constant for $ONOO^-$ crossing lipid bilayers was found to be $k_{D,4} = 320$ s^{-1}. Due to the acid–base equilibrium between $ONOO^-$ and its conjugated acid $ONOOH$, this is likely an average value for $ONOO^-$ and $ONOOH$. Thus, $k_{D,7} = k_{D,4} = 320$ s^{-1}. Since NO_2^- is an anion as well as similar in size, we assume the same value (i.e., $k_{D,4} = k_{D,5}$). The used diffusion rate constants are summarized in Table 6. Note that we do not consider the potential effect of the PTL on the membrane diffusion rate constants in our model.

Table 6. Membrane diffusion rate constants.

Rate Constant	Parameter Value	Reference	Remark
$k_{D,4}$	320 s^{-1}	[96]	
$k_{D,5}$	320 s^{-1}		Assigned
$k_{D,7}$	320 s^{-1}	[96]	

6.2.3. Initial Concentrations

The used initial concentrations in the EC and IC are summarized in Tables 7 and 8, respectively.

Table 7. Initial concentrations of the species in the extracellular compartment.

Species	Initial Concentration (*M*)	Reference	Remark
H_2O_2	Varied		
$ONOO^-$	0		Assigned
NO_2^-	Varied		
H^+	10^{-7}		Assigned
$ONOOH$	0		Assigned
CO_2	10^{-3}	[110]	

Table 8. Initial concentrations of the species in the intracellular compartment.

Species	Initial Concentration (*M*)	Reference	Remark
H_2O_2	Varied		
$CATFe^{III}$	Varied		
$CATFe^{IV}O^{\bullet+}$	0		Assigned
$ONOO^-$	0		Assigned
NO_2^-	10^{-4}	[111–113]	See Appendix D
H^+	10^{-7}		Assigned
$ONOOH$	0		Assigned
CO_2	10^{-3}	[110]	See Appendix D

The initial concentration of intracellular H_2O_2 (i.e., $c_{1,0}^{IC}$) is varied with the initial concentration of catalase in order to achieve the correct steady-state $c_{1,0}^{IC}$ for each $[CATFe^{III}]_0$. The H_2O_2 generation from mitochondria is in the range of 50 µmol kg^{-1} min^{-1} [114], which corresponded to $k_P = 1 \times 10^{-7}$ Ms^{-1} [115].

Thus, from Equation (10), at t = 0 (and thus, the term $k_{D,1}\left(c_1^{EC} - c_1^{IC}\right)$ vanishes),

$$\frac{dc_1^{IC}}{dt} = -k_1 c_1^{IC} c_2 - k_2 c_1^{IC} c_3 - k_3 c_1^{IC} c_5^{IC} c_6^{IC} + k_P = 0.$$

Assuming that $c_3 = 0$ at steady-state,

$$k_P = c_{1,ss}^{IC}\left(k_1 c_2 + k_3 c_5^{IC} c_6^{IC}\right) \Leftrightarrow$$

$$c_{1,ss}^{IC} = \frac{k_P}{\left(k_1 c_2 + k_3 c_5^{IC} c_6^{IC}\right)}. \quad (18)$$

Hence, $c_{1,ss}^{IC} = c_{1,0}^{IC}$ in our model.

6.3. Software and Details about the Calculations

The numerical calculations are performed in MATLAB. Due to significant differences in time scales, we use the solver ode23s to solve the set of rate equations.

The simulations are performed at time-scales covering the transient of the system's response. For the calculations, we use the time intervals and time steps shown in Table 9. We start with a very short time-step in the first 10 ms, which is then enlarged by a factor of 100 until 1 s, and again by a factor of 100 until the final time of 100 s.

Table 9. Time intervals and time steps.

Time	Value (s)	Time Step	Value (s)
t_1	10^{-2}	dt_1	10^{-7}
t_2	1	dt_2	10^{-5}
t_f	10^2	dt_3	10^{-3}

We furthermore vary the independent variables according to Table 10.

Table 10. Minimal and maximal values as well as number of steps of independent variables.

Independent Variable	Minimal Value	Maximal Value	Number of Steps
$[CATFe^{III}]$	10^{-8} M	10^{-5} M	100
$k_{D,1}$	100 s^{-1}	2000 s^{-1}	100

7. Conclusions

With this study, we aim to gain insights about the possible mechanisms underlying the anti-cancer effect of plasma-treated liquids (PTLs). In particular, we are interested in whether cell susceptibility toward PTL can be quantified in terms of cell-specific features, how selectivity arises, and why H_2O_2 combined with NO_2^- (as in PTL) offers a synergistic and thus enhanced anti-cancer effect compared with H_2O_2 only. By developing a mathematical model describing the kinetics of the species in PTL-treated cells, we analyze four different dependent variables as a function of the H_2O_2 membrane diffusion rate constant and the intracellular catalase concentration. Ultimately, one or more of these dependent variables could be used to quantify selective and synergistic effects of PTLs for different types of cells. In accordance with experimental observations, cancer cells are supposed to be associated with a higher H_2O_2 membrane diffusion rate constant and a lower intracellular catalase concentration compared to normal cells, and we use this knowledge in the evaluation of our proposed dependent variables.

The model is built up *ab initio* based on the species, reactions, and processes of major importance in the context of cell susceptibility toward PTL, and parameter values such as rate constants are extracted from the literature. Thus, the model itself summarizes the current state of knowledge on the matter in a compact and descriptive manner. This type of mathematical modeling to gain insight into the underlying mechanisms of the anti-cancer effect of PTL is novel and this study is the first of its kind in the field of plasma oncology. Furthermore, we propose new ways to quantify the selective and synergistic anti-cancer effect of PTL in terms of inherent cell features, which is also an innovative approach in the ongoing research on the mode of action of PTL.

We find that the temporal maximal intracellular H_2O_2 concentration shows a dependency of the H_2O_2 membrane diffusion rate constant and the intracellular catalase concentration, so that it could possibly be used to quantify the anti-cancer effect of exogenous H_2O_2, but it does not account for the synergistic effect of H_2O_2 and NO_2^- in PTL. However, by including the reactions where $CO_3^{\bullet -}$ is produced in the CO_2 catalyzed consumption of $ONOO^-$, and the interaction between $CO_3^{\bullet -}$ and catalase, the dependent variable $c_{1,\max}$ could possibly also be able to account for the synergetic effect of NO_2^-.

We believe that our model is an important step to unveil the underlying mechanisms of the anti-cancer effect of CAP and PTLs, but more efforts are needed in order to understand the full picture of the causes and action. Here, both positive and negative results are important to share, in order to increase our collective knowledge of which clues may lead us forward in our search, and which clues we can leave behind, at least for now. Theoretical and experimental approaches to investigate possible key features of cells and their interaction with CAP and PTLs play complementary roles in our aim to push the limit of knowledge further. We hope, and believe, that our study contributes to the quest to quantify selective and synergistic effects of plasma for cancer treatment.

Author Contributions: Conceptualization, C.B.; Methodology, C.B.; Software, C.B.; Validation, C.B. and A.B.; Formal analysis, C.B.; Investigation, C.B.; Resources, A.B.; Data curation, C.B.; Writing—original draft preparation, C.B.; Writing—review and editing, C.B. and A.B.; Visualization, C.B.; Supervision, A.B.; Project administration, C.B.; Funding acquisition, A.B. All authors have read and agreed to the published version of the manuscript.

Funding: This research received no external funding.

Conflicts of Interest: The authors declare no conflict of interest. The funders had no role in the design of the study; in the collection, analyses, or interpretation of data; in the writing of the manuscript, or in the decision to publish the results.

Appendix A. Additional Results

Appendix A.1. Temporal Maximum of the Intracellular Peroxynitrite Concentration

Figure A1 shows the result for the dependent variable $c_{4,max}$ for $[H_2O_2]_0^{EC} = 1$ µM, with and without NO_2^-. The same results, but for $[H_2O_2]_0^{EC} = 1$ mM, are shown in Figure A2.

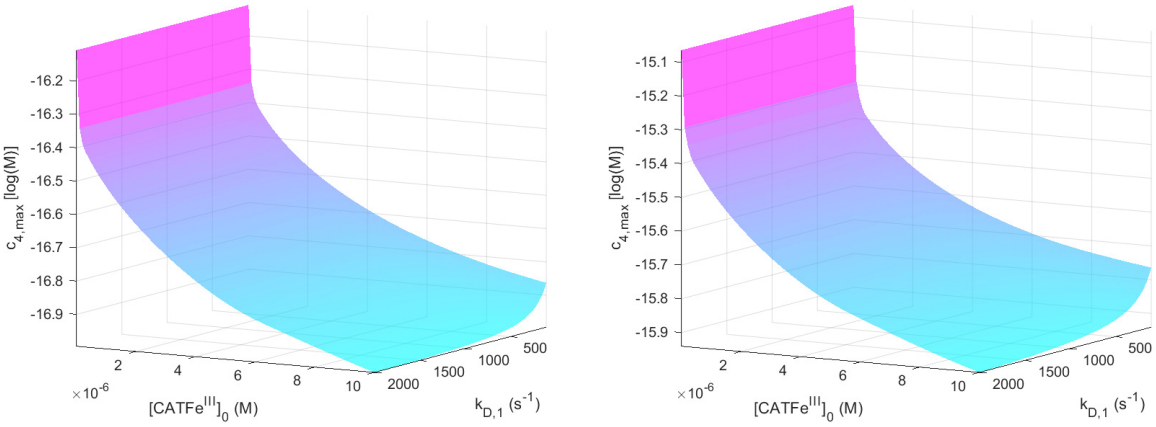

(**a**) (**b**)

Figure A1. The dependent variable $c_{4,max}$ (i.e., the temporal maximum of $[ONOO^-]$ in the IC) as a function of $k_{D,1}$ and $[CATFe^{III}]_0$ when $[H_2O_2]_0^{EC} = 1$ µM. $[NO_2^-]_0^{EC} = 0$ M (**a**) and $[NO_2^-]_0^{EC} = 1$ mM (**b**).

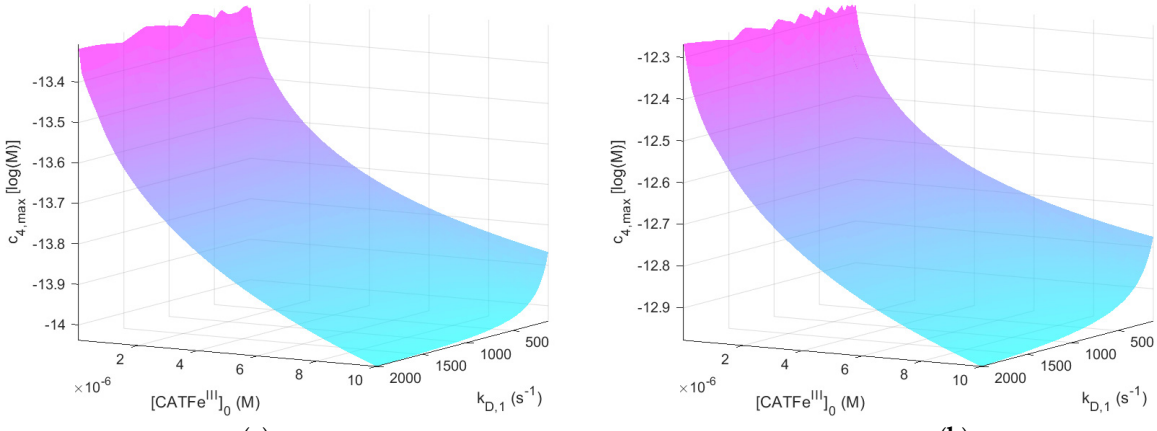

(**a**) (**b**)

Figure A2. The dependent variable $c_{4,max}$ (i.e., the temporal maximum of $[ONOO^-]$ in the IC) as a function of $k_{D,1}$ and $[CATFe^{III}]_0$ when $[H_2O_2]_0^{EC} = 1$ mM. $[NO_2^-]_0^{EC} = 0$ M (**a**) and $[NO_2^-]_0^{EC} = 1$ mM (**b**).

The dependent variable $c_{4,max}$ could account for selectivity with respect to the different regimes of $[H_2O_2]_0^{EC}$ in the same manner as $c_{1,max}$ (see Figures A1a and A2a ($c_{4,max}$) and Figures 2a and 3a ($c_{1,max}$)). Indeed, there is a difference in $c_{4,max}$ of about three orders

of magnitude for $[H_2O_2]_0^{EC} = 1$ mM (Figure A2a) compared with $[H_2O_2]_0^{EC} = 1$ µM (Figure A1a).

When comparing Figure A1a,b, we see that although the overall behavior of $c_{4,\max}$ is very similar, there is an order of magnitude difference in its value. In other words, the addition of NO_2^- increases the value of $c_{4,\max}$ for all $k_{D,1}$ and $[CATFe^{III}]_0$. Thus, $c_{4,\max}$ could account for the observed synergetic effect of PTL.

We see that for $[H_2O_2]_0^{EC} = 1$ µM (Figure A1a), $c_{4,\max}$ shows a clear $[CATFe^{III}]_0$-dependence and is relatively independent of $k_{D,1}$ for low $[CATFe^{III}]_0$. However, the $k_{D,1}$-dependence gradually increases with increasing $[CATFe^{III}]_0$. In this case, the dependence is such that $c_{4,\max}$ (for a given value of $[CATFe^{III}]_0$) is inversely dependent on $k_{D,1}$. This is not consistent with the pattern we are looking for and although the formation of intracellular $ONOO^-$ could play a role in the overall cytotoxicity of PTL, we do not believe that it plays the main role. In this context, it should also be noted that even the maximal amount formed corresponds to a very low concentration.

In summary, the dependent variable $c_{4,\max}$ could account for selectivity with respect to the concentration of H_2O_2 as well as the synergistic effect of PTLs. Indeed, the addition of NO_2^- in the extracellular compartment does increase $c_{4,\max}$ with about one order of magnitude. This could, however, be expected since the formation of $ONOO^-$ is directly proportional to the concentration of NO_2^- and with $[NO_2^-]_0^{EC} = 10[NO_2^-]_0^{IC}$, the intracellular concentration of NO_2^- will increase with about one order of magnitude compared to when no extracellular NO_2^- is added. Still, $c_{4,\max}$ does not show a dependency that is consistent with a measure of the cell susceptibility toward PTL. However, as we discuss in Sections 4 and 7, instead, by using the temporal maximum of intracellular $[CO_3^{\bullet -}]$, which is produced in the CO_2-catalyzed decomposition of $ONOO^-$, as a dependent variable, a feasible measure could possibly be found.

Appendix A.2. System Response Time of Intracellular Hydrogen Peroxide

Figure A3 shows the result for the dependent variable τ for $[H_2O_2]_0^{EC} = 1$ µM, with and without NO_2^-. The same results, but for $[H_2O_2]_0^{EC} = 1$ mM, are shown in Figure A4.

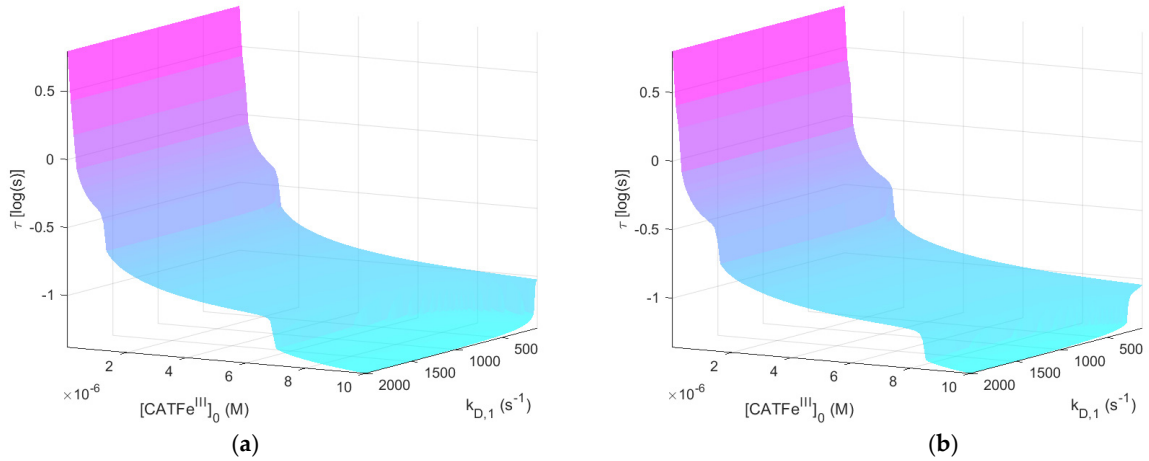

Figure A3. The dependent variable τ (i.e., the system response time of $[H_2O_2]$ in the IC) as a function of $k_{D,1}$ and $[CATFe^{III}]_0$ when $[H_2O_2]_0^{EC} = 1$ µM. $[NO_2^-]_0^{EC} = 0$ M (**a**) and $[NO_2^-]_0^{EC} = 1$ mM (**b**).

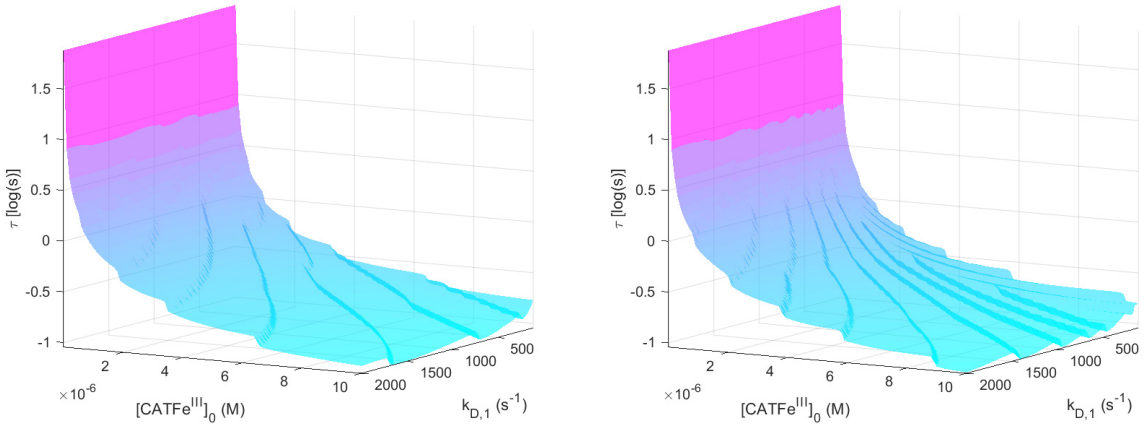

Figure A4. The dependent variable τ (i.e., the system response time of $[H_2O_2]$ in the IC) as a function of $k_{D,1}$ and $[CATFe^{III}]_0$ when $[H_2O_2]_0^{EC} = 1$ mM. $[NO_2^-]_0^{EC} = 0$ M (**a**) and $[NO_2^-]_0^{EC} = 1$ mM (**b**).

Here, the different concentration regimes of $[H_2O_2]_0^{EC}$ do not lead to well separated regimes of τ; in Figure A3a, we see that $-1.5 \lesssim \log(\tau) \lesssim 1$ whereas for $[H_2O_2]_0^{EC} = 1$ mM (Figure A4a), $-1 \lesssim \log(\tau) \lesssim 2$. Thus, τ is not a dependent variable that clearly takes into account selectivity with respect to $[H_2O_2]_0^{EC}$. Moreover, since the system response time is decreased with increased $[H_2O_2]_0^{EC}$, cells would then be less sensitive to higher concentrations of extracellular H_2O_2, which is not in accordance with the experimental observations.

However, there is a synergistic effect for a subspace of the total $k_{D,1}$, $[CATFe^{III}]_0$-space (see Figure A3a,b); in the region of high $[CATFe^{III}]_0$ and for approximately the whole $k_{D,1}$-regime, the addition of NO_2^- corresponds to an increased value of τ.

In Figure A3a, we see that τ is more or less independent of $k_{D,1}$; the overall dominant independent variable is $[CATFe^{III}]_0$. The $[CATFe^{III}]_0$-dependence is such that the decrease of τ for increased $[CATFe^{III}]_0$ has regions with distinct drops of τ in the overall exponential decrease of τ. Moreover, there is a region at high $[CATFe^{III}]_0$ and low $k_{D,1}$ where there is a slight $k_{D,1}$-dependence. This dependence is such that if a longer response time is associated with higher susceptibility, in a certain region of $k_{D,1}$, a higher value of $k_{D,1}$ has a protective effect compared to a lower value of $k_{D,1}$ (for a constant $[CATFe^{III}]_0$). This effect is increased when NO_2^- is added to the system. Since this does not correspond to the current state of knowledge (see Section 2.1), the system response time does not seem like a suitable dependent variable to quantify the cellular response to H_2O_2 and NO_2^-.

In summary, the system response time, τ, does not seem to be a suitable measure to quantify the cell susceptibility toward PTL.

Appendix A.3. Load of Intracellular Hydrogen Peroxide and Peroxynitrite

Figure A5 shows the result for the dependent variable l_1 for $[H_2O_2]_0^{EC} = 1$ µM, with and without NO_2^-. The same results, but for $[H_2O_2]_0^{EC} = 1$ mM, are shown in Figure A6.

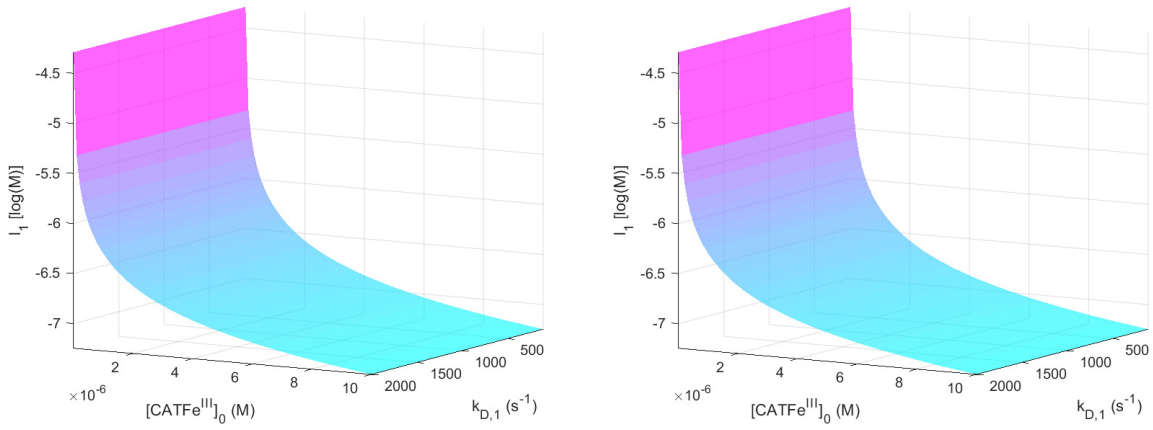

(**a**) (**b**)

Figure A5. The dependent variable l_1 (i.e., the load of H_2O_2 in the IC) as a function of $k_{D,1}$ and $[CATFe^{III}]_0$ when $[H_2O_2]_0^{EC} = 1$ µM. $[NO_2^-]_0^{EC} = 0$ M (**a**) and $[NO_2^-]_0^{EC} = 1$ mM (**b**).

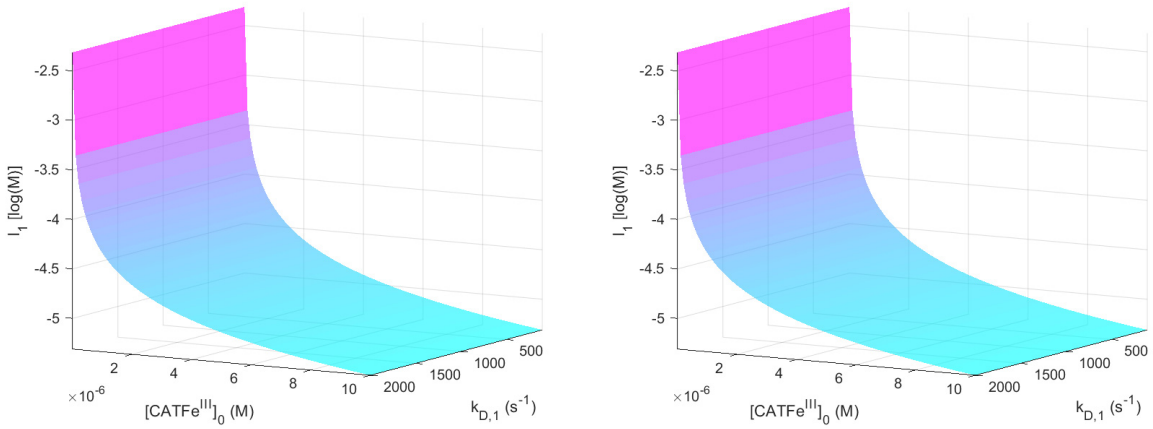

(**a**) (**b**)

Figure A6. The dependent variable l_1 (i.e., the load of H_2O_2 in the IC) as a function of $k_{D,1}$ and $[CATFe^{III}]_0$ when $[H_2O_2]_0^{EC} = 1$ mM. $[NO_2^-]_0^{EC} = 0$ M (**a**) and $[NO_2^-]_0^{EC} = 1$ mM (**b**).

Likewise, Figure A7 shows the results for the dependent variable $l_{1,BS}$ for $[H_2O_2]_0^{EC} = 1$ µM, with and without NO_2^-. The same results, but for $[H_2O_2]_0^{EC} = 1$ mM, are shown in Figure A8.

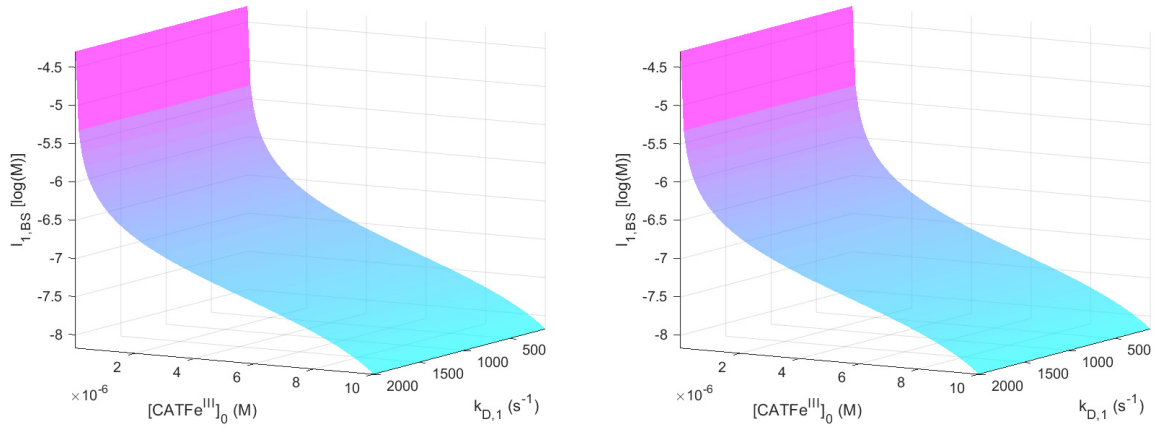

(**a**) (**b**)

Figure A7. The dependent variable $l_{1,BS}$ (i.e., the load over the baseline of H_2O_2 in the IC) as a function of $k_{D,1}$ and $[CATFe^{III}]_0$ when $[H_2O_2]_0^{EC} = 1$ µM. $[NO_2^-]_0^{EC} = 0$ M (**a**) and $[NO_2^-]_0^{EC} = 1$ mM (**b**).

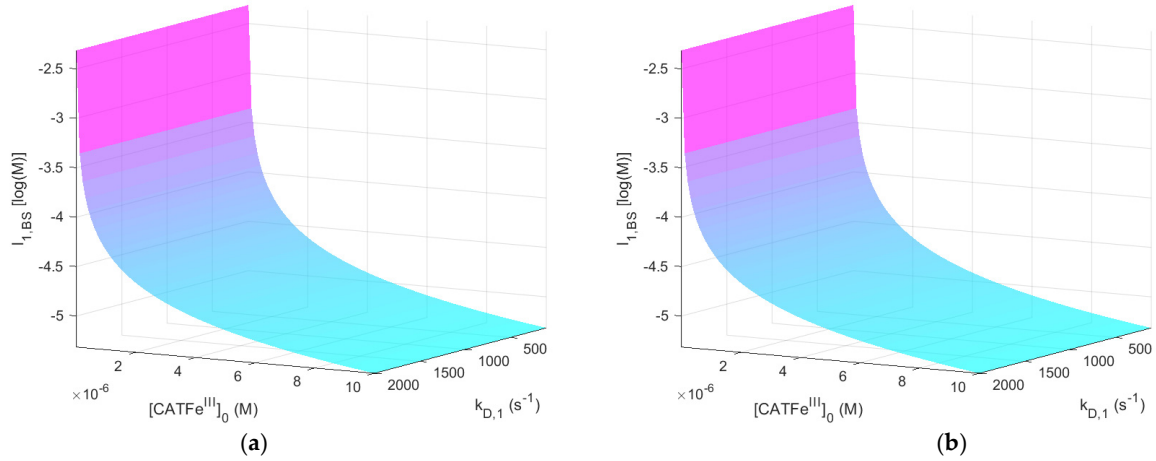

Figure A8. The dependent variable $l_{1,BS}$ (i.e., the load over the baseline of H_2O_2 in the IC) as a function of $k_{D,1}$ and $[CATFe^{III}]_0$ when $[H_2O_2]_0^{EC} = 1$ mM. $[NO_2^-]_0^{EC} = 0$ M (**a**) and $[NO_2^-]_0^{EC} = 1$ mM (**b**).

If one excludes the systems with the lowest levels of $[CATFe^{III}]_0$, l_1 could account for the selectivity with respect to different $[H_2O_2]_0^{EC}$; when comparing Figures A5a and A6a, there is a region for which $-7.5 \lesssim \log(l_1) \lesssim -5.5$ for $[H_2O_2]_0^{EC} = 1$ µM, whereas in the same region, $-5.5 \lesssim \log(l_1) \lesssim -3.5$ for $[H_2O_2]_0^{EC} = 1$ mM. The very same situation applies for $l_{1,BS}$; by excluding the lowest regime of $[CATFe^{III}]_0$, selectivity with respect to different $[H_2O_2]_0^{EC}$ could be taken into account (see Figures A7a and A8a).

When comparing Figure A5a,b, there is no observable effect on l_1 when adding NO_2^- into the system. Thus, l_1 does not seem to take the synergistic effect into account. The same situation applies for $l_{1,BS}$.

In Figure A5a, we see that l_1 is independent of $k_{D,1}$ and only dependent on $[CATFe^{III}]_0$. Thus, l_1 is not suitable as a measure to quantify cell susceptibility in terms of both $k_{D,1}$ and $[CATFe^{III}]_0$. From Figure A7a, we see that $l_{1,BS}$ differs a bit from l_1; $l_{1,BS}$ is less sensitive to an increased $[CATFe^{III}]_0$ at low $[CATFe^{III}]_0$ in particular. In addition, there is a point of inflection somewhere along the $[CATFe^{III}]_0$-axis (i.e., the graph is initially concave up and then shifts to concave down). This means that the rate of change of $l_{1,BS}$ with respect to $[CATFe^{III}]_0$ changes from increasing to decreasing somewhere on the $[CATFe^{III}]_0$-axis. Nevertheless, $l_{1,BS}$ is still independent of $k_{D,1}$, and thus it does not represent a feasible measure to quantify the cell susceptibility toward PTL.

Figure A9 shows the result for the dependent variable l_4 for $[H_2O_2]_0^{EC} = 1$ µM, with and without NO_2^-. The same results, but for $[H_2O_2]_0^{EC} = 1$ mM, are shown in Figure A10.

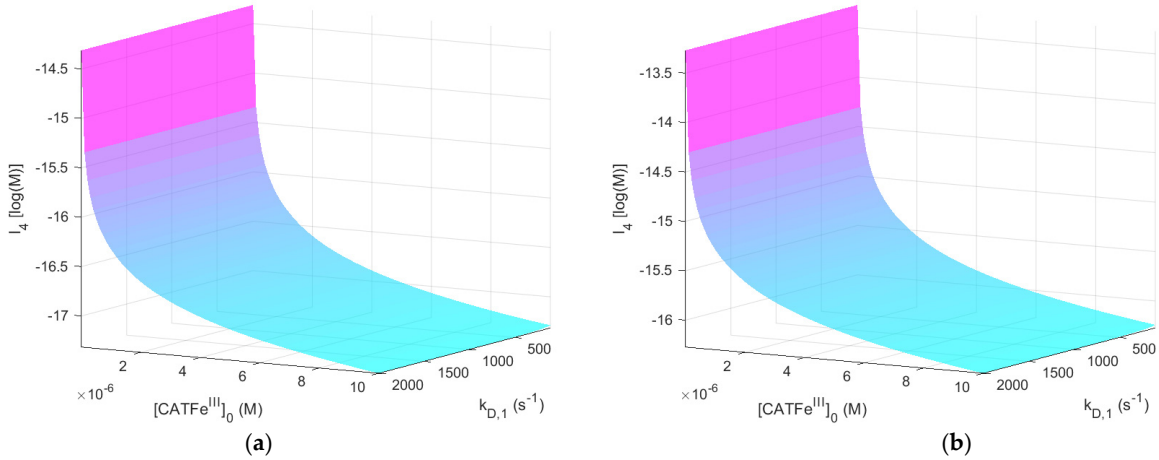

Figure A9. The dependent variable l_4 (i.e., the load of $ONOO^-$ in the IC) as a function of $k_{D,1}$ and $[CATFe^{III}]_0$ when $[H_2O_2]_0^{EC} = 1$ µM. $[NO_2^-]_0^{EC} = 0$ M (**a**) and $[NO_2^-]_0^{EC} = 1$ mM (**b**).

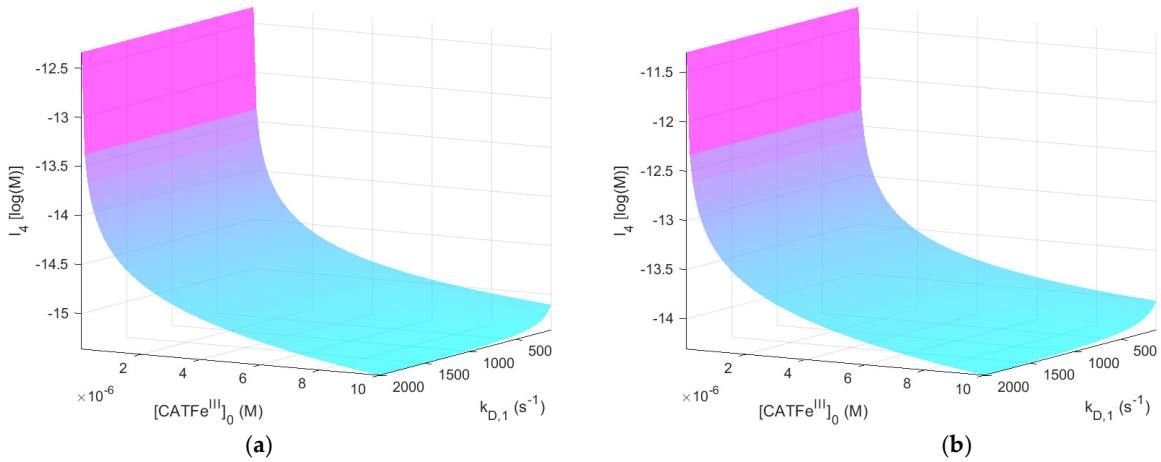

Figure A10. The dependent variable l_4 (i.e., the load of $ONOO^-$ in the IC) as a function of $k_{D,1}$ and $[CATFe^{III}]_0$ when $[H_2O_2]_0^{EC} = 1$ mM. $[NO_2^-]_0^{EC} = 0$ M (**a**) and $[NO_2^-]_0^{EC} = 1$ mM (**b**).

The pattern for l_4 more or less follows the same pattern as for l_1 selectivity with respect to $[H_2O_2]_0^{EC}$ is only taken into account if the $[CATFe^{III}]_0$-regime is modified by removing the lowest levels of $[CATFe^{III}]_0$. In addition, l_4 is independent of $k_{D,1}$ and thus, it does not represent a feasible measure for quantifying cell-susceptibility. However, there exists a synergistic effect; l_4 is about one order of magnitude higher at every point in the $(k_{D,1}, [CATFe^{III}]_0)$-space when NO_2^- is added.

In summary, looking for a variable that depends on both $[CATFe^{III}]_0$ and $k_{D,1}$, none of the dependent variables l_1, l_4, or $l_{1,BS}$ seem to be appropriate candidates for a dependent variable able to capture and quantify the cell susceptibility toward PTL.

Appendix A.4. Rate of Extracellular Hydrogen Peroxide Consumption

Figure A11 shows the result for the dependent variable $\bar{s}$ for $[H_2O_2]_0^{EC} = 1$ µM, with and without NO_2^-. The same results, but for $[H_2O_2]_0^{EC} = 1$ mM, are shown in Figure A12.

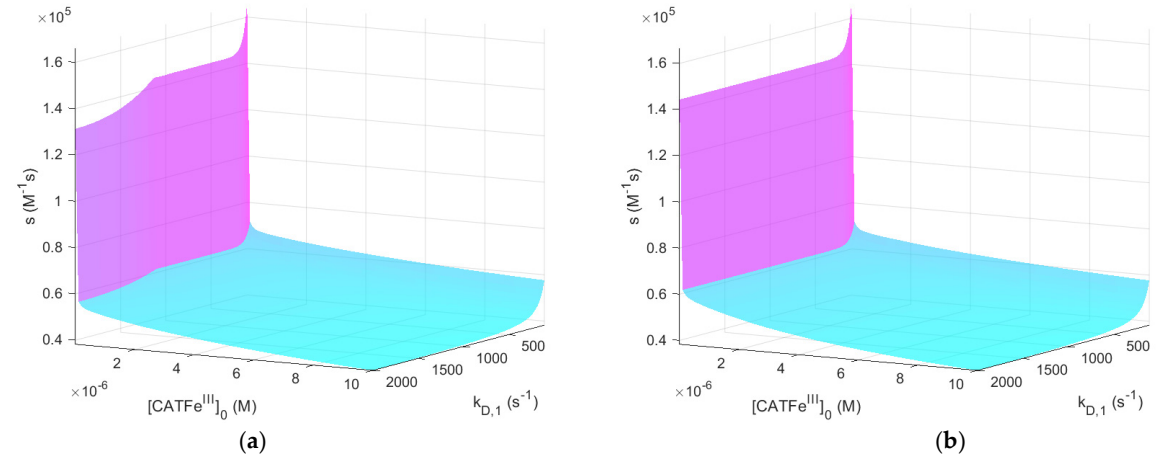

Figure A11. The dependent variable $\bar{s}$ (i.e., the inverse of the average rate of H_2O_2 consumption in the EC) as a function of $k_{D,1}$ and $[CATFe^{III}]_0$ when $[H_2O_2]_0^{EC} = 1$ µM. $[NO_2^-]_0^{EC} = 0$ M (**a**) and $[NO_2^-]_0^{EC} = 1$ mM (**b**).

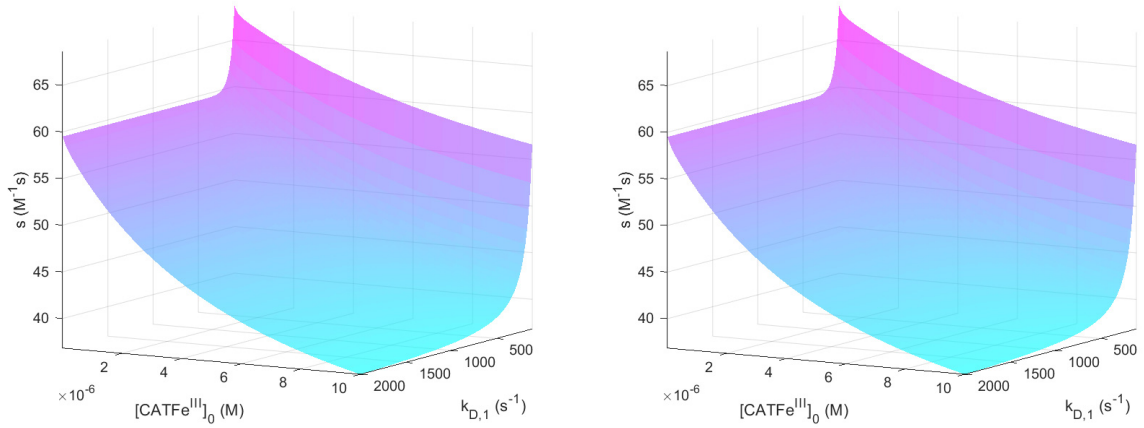

Figure A12. The dependent variable $\bar{s}$ (i.e., the inverse of the average rate of H_2O_2 consumption in the EC) as a function of $k_{D,1}$ and $[CATFe^{III}]_0$ when $[H_2O_2]_0^{EC} = 1$ mM. $[NO_2^-]_0^{EC} = 0$ M (**a**) and $[NO_2^-]_0^{EC} = 1$ mM (**b**).

Here, one has to be a bit careful to compare $\bar{s}$ for different regimes of $[H_2O_2]_0^{EC}$. Obviously, a larger value of $[H_2O_2]_0^{EC}$ will correspond to a higher membrane diffusion rate of H_2O_2 from the EC to the IC, which will affect the consumption rate so that it increases with increasing H_2O_2 membrane diffusion rate. When comparing $\bar{s}$ for $[H_2O_2]_0^{EC} = 1$ µM (Figure A11a) and for $[H_2O_2]_0^{EC} = 1$ mM (Figure A12a), we see that it is many orders of magnitude higher in the latter case, even though we know that $[H_2O_2]_0^{EC} = 1$ mM is associated with a higher cytotoxic effect than $[H_2O_2]_0^{EC} = 1$ µM. Thus, for this choice of dependent variable, it is not meaningful to compare the results for different regimes of $[H_2O_2]_0^{EC}$; in other words, selectivity with respect to $[H_2O_2]_0^{EC}$ cannot be verified.

For the potential synergistic effect, we see in Figure A11 that even though there is a slight deviation of Figure A11a compared to Figure A11b for very low values of $[CATFe^{III}]_0$, it is not enough to verify a synergistic effect when NO_2^- is added to the system.

The variable $\bar{s}$ is strongly dependent on $[CATFe^{III}]_0$ in the regime of very low values of $[CATFe^{III}]_0$. Here, the dependence is such that is could capture specific cell susceptibility in terms of $[CATFe^{III}]_0$. However, for larger values of $[CATFe^{III}]_0$, $\bar{s}$ is more or less constant and moreover, the very weak $k_{D,1}$-dependence is reverse to what would be expected (see Section 2.1). Thus, $\bar{s}$ does not seem to represent a feasible measure to quantify cell susceptibility in terms of $k_{D,1}$ and $[CATFe^{III}]_0$.

Finally, Figure A13 shows the result for the dependent variable $s_{\max}$ for $[H_2O_2]_0^{EC} = 1$ µM, with and without NO_2^-. The same results, but for $[H_2O_2]_0^{EC} = 1$ mM, are shown in Figure A14.

As for $\bar{s}$, we cannot compare $s_{\max}$ for different regimes of $[H_2O_2]_0^{EC}$ (see Figures A13a and A14a), so again the feature of selectivity with respect to $[H_2O_2]_0^{EC}$ cannot be verified. Furthermore, there is no observable synergistic effect when NO_2^- is added to the system (see Figure A13a,b).

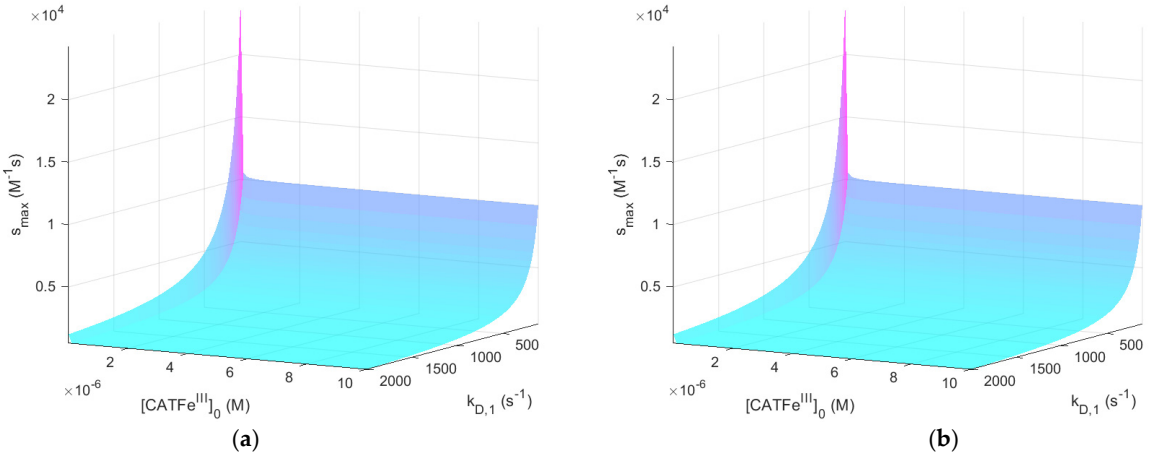

Figure A13. The dependent variable $s_{\max}$ (i.e., the inverse of the maximal rate of H_2O_2 consumption in the EC) as a function of $k_{D,1}$ and $[CATFe^{III}]_0$ when $[H_2O_2]_0^{EC} = 1$ µM. $[NO_2^-]_0^{EC} = 0$ M (**a**) and $[NO_2^-]_0^{EC} = 1$ mM (**b**).

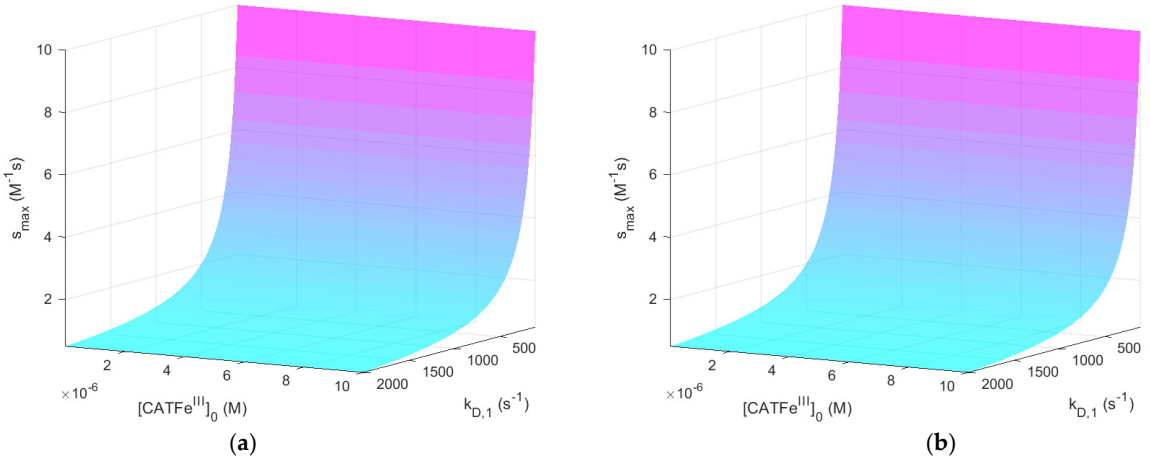

Figure A14. The dependent variable $s_{\max}$ (i.e., the inverse of the maximal rate of H_2O_2 consumption in the EC) as a function of $k_{D,1}$ and $[CATFe^{III}]_0$ when $[H_2O_2]_0^{EC} = 1$ mM. $[NO_2^-]_0^{EC} = 0$ M (**a**) and $[NO_2^-]_0^{EC} = 1$ mM (**b**).

Opposed to $\bar{s}$, $s_{\max}$ is more or less independent of $[CATFe^{III}]_0$ and only dependent of $k_{D,1}$. However, the dependence of $k_{D,1}$ is reverse to what would be expected (see Section 2.1); the lower value of $k_{D,1}$, the higher cell susceptibility toward PTL. Thus, $s_{\max}$ does not qualify as a measure to quantify the cell susceptibility in terms of $k_{D,1}$ and $[CATFe^{III}]_0$.

In summary, neither $\bar{s}$ or $s_{\max}$ seem to be appropriate candidates for a dependent variable able to capture and quantify the cell response to PTL.

Appendix B. Derivation of the Rate of Diffusion Equation

According to Fick's first law, the flow of a species through a membrane can be written as

$$J = \frac{1}{A}\frac{dn}{dt} = -D\frac{dc}{dx}, \tag{A1}$$

where J denotes the flow in mol $m^{-2}s^{-1}$; A is the surface area of the membrane (m^{-2}); n is the amount of the substance (mol); D is the diffusion coefficient (m^2s^{-1}); c is the concentration (M). By assuming a linear concentration gradient over the cell membrane, we can write

$$\frac{dc}{dx} = \frac{c_2 - c_1}{\Delta x}, \tag{A2}$$

where Δx is the width of the membrane, see Figure A15, Equations (A1) and (A2) yields

$$\frac{dn}{dt} = -\frac{DA}{\Delta x}(c_2 - c_1), \tag{A3}$$

$$\Leftrightarrow \frac{1}{V}\frac{dn}{dt} = -\frac{DA}{V\Delta x}(c_2 - c_1), \tag{A4}$$

where V denotes the encapsulated volume (m^3). Here, it is a custom to define the term

$$P = \frac{D}{\Delta x}, \tag{A5}$$

as the permeability of the membrane. In these terms, Equation (A4) can be written as

$$\frac{dc}{dt} = \frac{-AP}{V}(c_2 - c_1). \tag{A6}$$

Thus, in our Equation (2) in the main paper,

$$k_D = \frac{-AP}{V}. \tag{A7}$$

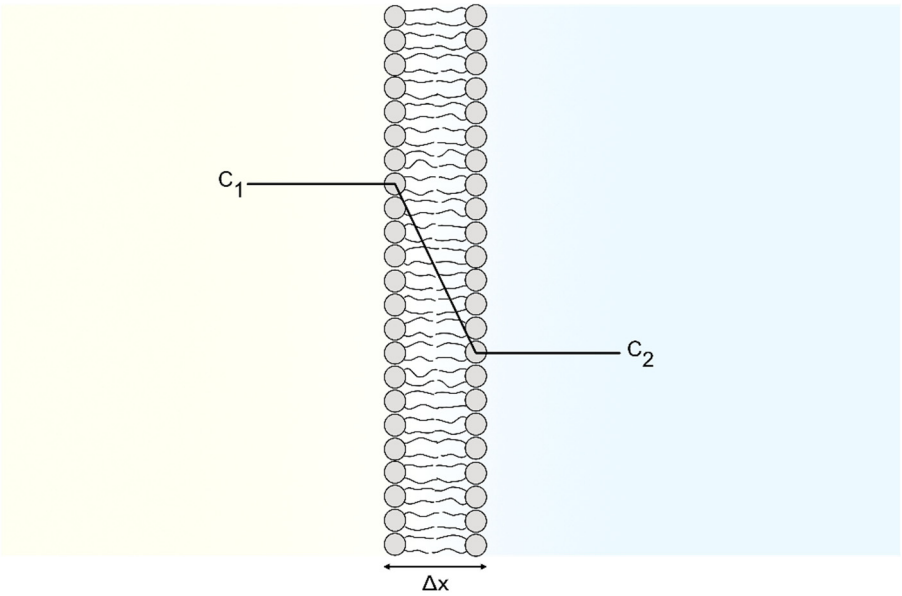

Figure A15. Illustration of a linear concentration gradient over a membrane.

Appendix C. Estimates of Intracellular Catalase Concentration

Appendix C.1. Catalase Concentration Corresponding to a Normal Steady-State Concentration of Hydrogen Peroxide

H_2O_2 is continuously produced in vivo [103] and remains in a quasi-steady-state. Normal intracellular steady-state concentrations of H_2O_2 are 10 nM or less [103,116].

Assuming that the mitochondria are the major source of intracellular H_2O_2, and that catalase is the only enzyme responsible for its decomposition, we estimate the average intracellular concentration of catalase. Denoting $x = [H_2O_2]$, $y = \left[CATFe^{III}\right]$, and $z = \left[CATFe^{IV}O^{\bullet+}\right]$, and including the constraint that $z = y_0 - y$, the rate equation for x is

$$\frac{dx}{dt} = -x(k_1 y + k_2(y_0 - y)) + k_P. \tag{A8}$$

Denoting the steady state concentration of H_2O_2 as x_{ss}, Equation (A8) yields

$$-x_{ss}(k_1 y + k_2(y_0 - y)) + k_P = 0 \Rightarrow$$

$$y_0 = -y\left(\frac{k_1}{k_2} - 1\right) + \frac{k_P}{k_2 x_{ss}}, \quad \text{(A9)}$$

in other words, the solutions are found on the straight line given by Equation (A9). For example, $y = y_0$ ($x_{ss} \sim 10^{-8}$ M),

$$y_0 = \frac{k_P}{k_1 x_{ss}} \sim 6 \times 10^{-7} \text{ M}.$$

Appendix C.2. Catalase Concentration from Detected Catalase Monomers per Cell

In [62], the effective number of fully active catalase monomers per cell for various cancer cell lines was detected. This number varied from 101×10^3 to 538×10^3 and there was a strong correlation between the rate constant of H_2O_2-decomposition and the number of fully active catalase monomers per cell. Since each catalase molecule consists of four monomers, the number of catalase molecules per cell is thus roughly $(25–125) \times 10^3$. The conclusions in [62] were that the rate constant for removal of extracellular H_2O_2 were on average two times higher in normal cells than in cancer cells, and that catalase activity is critical in removing this H_2O_2. If normal cells have a capacity that is twice as large to remove H_2O_2, the number of catalase molecules for the cancer cell lines' normal counterparts should be $(50–250) \times 10^3$. If N denotes the number of molecules per cell, the number of moles per cell is

$$n = \frac{N}{N_A},$$

where

$$N_A \sim 6.022 \times 10^{23} \text{ mol}^{-1},$$

is Avogadro's number. If each cell can be assumed to be a sphere of radius $r \sim 20$ μM (as has been estimated for HeLa-cells [117]), its volume is given by

$$V = \frac{4\pi}{3} r^3.$$

Thus, the average concentration of catalase per cell is

$$\left[CATFe^{III}\right] = \frac{n}{V}.$$

For $N = 100 \times 10^3$, $\left[CATFe^{III}\right] \sim 6 \times 10^{-6}$ M.

Appendix D. Concentration of Intracellular Nitrite and Carbon Dioxide

The NO_2^--levels measured in human physiological fluids are 0.5–210 μM [111–113].

The partial pressure in human alveolar has been found to be $p_{CO_2} = (4.0–9.3) \times 10^3$ Pa [110], which according to Henry's law yields $[CO_2] = Hp$, where $H = 3.4 \times 10^{-2}$ M atm^{-1} is Henry's constant for CO_2 in water at $T = 298.15$ K (i.e., $[CO_2] = (1.3–3.1) \times 10^{-3}$ M). Cell culture media (Eagle's) contained 2200 mgL^{-1} of $NaHCO_3$ (i.e., $\left[HCO_3^-\right] = 36$ mM). At $pH = 7.0$, this corresponds to $[CO_2] = 36$ mM.

References

1. Privat-Maldonado, A.; Bengtson, C.; Razzokov, J.; Smits, E.; Bogaerts, A. Modifying the tumour microenvironment: Challenges and Future Perspectives for Anticancer Plasma Treatments. *Cancers* **2019**, *11*, 1920. [CrossRef]
2. Van Boxem, W.; Van der Paal, J.; Gorbanev, Y.; Vanuytsel, S.; Smits, E.; Dewilde, S.; Bogaerts, A. Anti-cancer capacity of plasma-treated PBS: Effect of chemical composition on cancer cell cytotoxicity. *Sci. Rep.* **2017**, *7*, 15. [CrossRef]

3. Lin, A.; Truong, B.; Patel, S.; Kaushik, N.; Choi, E.H.; Fridman, G.; Fridman, A.; Miller, V. Nanosecond-Pulsed DBD plasma-generated reactive oxygen species trigger immunogenic cell death in A549 lung carcinoma cells through intracellular oxidative stress. *Int. J. Mol. Sci.* **2017**, *18*, 966. [CrossRef] [PubMed]
4. Lin, A.; Gorbanev, Y.; De Backer, J.; Van Loenhout, J.; Van Boxem, W.; Lemiere, F.; Cos, P.; Dewilde, S.; Smits, E.; Bogaerts, A. Non-thermal plasma as a unique delivery system of short-lived reactive oxygen and nitrogen species for immunogenic cell death in melanoma cells. *Adv. Sci.* **2019**, *6*, 15. [CrossRef] [PubMed]
5. Bisag, A.; Bucci, C.; Coluccelli, S.; Girolimetti, G.; Laurita, R.; De Iaco, P.; Perrone, A.M.; Gherardi, M.; Marchio, L.; Porcelli, A.M.; et al. Plasma-activated Ringer's Lactate solution displays a selective cytotoxic effect on ovarian cancer cells. *Cancers* **2020**, *12*, 476. [CrossRef] [PubMed]
6. Biscop, E.; Lin, A.; Van Boxem, W.; Van Loenhout, J.; De Backer, J.; Deben, C.; Dewilde, S.; Smits, E.; Bogaerts, A. The influence of cell type and culture medium on determining cancer selectivity of cold atmospheric plasma treatment. *Cancers* **2019**, *11*, 1287. [CrossRef]
7. Bekeschus, S.; Freund, E.; Spadola, C.; Privat-Maldonado, A.; Hackbarth, C.; Bogaerts, A.; Schmidt, A.; Wende, K.; Weltmann, K.D.; von Woedtke, T.; et al. Risk Assessment of kINPen plasma treatment of four human pancreatic cancer cell lines with respect to metastasis. *Cancers* **2019**, *11*, 1237. [CrossRef] [PubMed]
8. Schuster, M.; Seebauer, C.; Rutkowski, R.; Hauschild, A.; Podmelle, F.; Metelmann, C.; Metelmann, B.; von Woedtke, T.; Hasse, S.; Weltmann, K.D.; et al. Visible tumor surface response to physical plasma and apoptotic cell kill in head and neck cancer. *J. Cranio-Maxillo-Facial Surg.* **2016**, *44*, 1445–1452. [CrossRef] [PubMed]
9. Metelmann, H.R.; Seebauer, C.; Miller, V.; Fridman, A.; Bauer, G.; Graves, D.B.; Pouvesle, J.M.; Rutkowski, R.; Schuster, M.; Bekeschus, S.; et al. Clinical experience with cold plasma in the treatment of locally advanced head and neck cancer. *Clin. Plasma Med.* **2018**, *9*, 6–13. [CrossRef]
10. Lim, J.B.; Huang, B.K.; Deen, W.M.; Sikes, H.D. Analysis of the lifetime and spatial localization of hydrogen peroxide generated in the cytosol using a reduced kinetic model. *Free Radic. Biol. Med.* **2015**, *89*, 47–53. [CrossRef]
11. Lim, J.B.; Langford, T.F.; Huang, B.K.; Deen, W.M.; Sikes, H.D. A reaction-diffusion model of cytosolic hydrogen peroxide. *Free Radic. Biol. Med.* **2016**, *90*, 85–90. [CrossRef]
12. Komalapriya, C.; Kaloriti, D.; Tillmann, A.T.; Yin, Z.K.; Herrero-de-Dios, C.; Jacobsen, M.D.; Belmonte, R.C.; Cameron, G.; Haynes, K.; Grebogi, C.; et al. Integrative Model of Oxidative Stress Adaptation in the Fungal Pathogen Candida albicans. *PLoS ONE* **2015**, *10*, e0137750.
13. Erudaitius, D.; Mantooth, J.; Huang, A.; Soliman, J.; Doskey, C.M.; Buettner, G.R.; Rodgers, V.G.J. Calculated cell-specific intracellular hydrogen peroxide concentration: Relevance in cancer cell susceptibility during ascorbate therapy. *Free Radic. Biol. Med.* **2018**, *120*, 356–367. [CrossRef]
14. Erudaitius, D.T.; Buettner, G.R.; Rodgers, V.G.J. The latency of peroxisomal catalase in terms of effectiveness factor for pancreatic and glioblastoma cancer cell lines in the presence of high concentrations of H_2O_2: Implications for the use of pharmacological ascorbate in cancer therapy. *Free Radic. Biol. Med.* **2020**, *156*, 20–25. [CrossRef] [PubMed]
15. Bengtson, C.; Bogaerts, A. On the anti-cancer effect of cold atmospheric plasma and the possible role of catalase-dependent apoptotic pathways. *Cells* **2020**, *9*, 2330. [CrossRef] [PubMed]
16. Ahn, H.J.; Kim, K.I.; Kim, G.; Moon, E.; Yang, S.S.; Lee, J.S. Atmospheric-pressure plasma jet induces apoptosis involving mitochondria via generation of free radicals. *PLoS ONE* **2011**, *6*, e28154. [CrossRef]
17. Arjunan, K.P.; Friedman, G.; Fridman, A.; Clyne, A.M. Non-thermal dielectric barrier discharge plasma induces angiogenesis through reactive oxygen species. *J. R. Soc. Interface* **2012**, *9*, 147–157. [CrossRef]
18. Yan, X.; Xiong, Z.L.; Zou, F.; Zhao, S.S.; Lu, X.P.; Yang, G.X.; He, G.Y.; Ostrikov, K. Plasma-Induced Death of HepG2 cancer cells: Intracellular effects of reactive species. *Plasma Process. Polym.* **2012**, *9*, 59–66. [CrossRef]
19. Ishaq, M.; Kumar, S.; Varinli, H.; Han, Z.J.; Rider, A.E.; Evans, M.D.M.; Murphy, A.B.; Ostrikov, K. Atmospheric gas plasma-induced ROS production activates TNF-ASK1 pathway for the induction of melanoma cancer cell apoptosis. *Mol. Biol. Cell* **2014**, *25*, 1523–1531. [CrossRef] [PubMed]
20. Kim, S.J.; Chung, T.H. Cold atmospheric plasma jet-generated RONS and their selective effects on normal and carcinoma cells. *Sci. Rep.* **2016**, *6*, 14. [CrossRef]
21. Kalghatgi, S.; Kelly, C.M.; Cerchar, E.; Torabi, B.; Alekseev, O.; Fridman, A.; Friedman, G.; Azizkhan-Clifford, J. Effects of non-thermal plasma on mammalian cells. *PLoS ONE* **2011**, *6*, e16270. [CrossRef]
22. Vandamme, M.; Robert, E.; Lerondel, S.; Sarron, V.; Ries, D.; Dozias, S.; Sobilo, J.; Gosset, D.; Kieda, C.; Legrain, B.; et al. ROS implication in a new antitumor strategy based on non-thermal plasma. *Int. J. Cancer* **2012**, *130*, 2185–2194. [CrossRef]
23. Van der Paal, J.; Neyts, E.C.; Verlackt, C.C.W.; Bogaerts, A. Effect of lipid peroxidation on membrane permeability of cancer and normal cells subjected to oxidative stress. *Chem. Sci.* **2016**, *7*, 489–498. [CrossRef] [PubMed]
24. Van der Paal, J.; Verheyen, C.; Neyts, E.C.; Bogaerts, A. Hampering effect of cholesterol on the permeation of reactive oxygen species through phospholipids bilayer: Possible explanation for plasma cancer selectivity. *Sci. Rep.* **2017**, *7*, 11. [CrossRef] [PubMed]
25. Girard, P.M.; Arbabian, A.; Fleury, M.; Bauville, G.; Puech, V.; Dutreix, M.; Sousa, J.S. Synergistic effect of H_2O_2 and NO_2 in cell death induced by cold atmospheric he plasma. *Sci. Rep.* **2016**, *6*, 17. [CrossRef] [PubMed]

26. Kurake, N.; Tanaka, H.; Ishikawa, K.; Kondo, T.; Sekine, M.; Nakamura, K.; Kajiyama, H.; Kikkawa, F.; Mizuno, M.; Hori, M. Cell survival of glioblastoma grown in medium containing hydrogen peroxide and/or nitrite, or in plasma-activated medium. *Arch. Biochem. Biophys.* **2016**, *605*, 102–108. [CrossRef] [PubMed]
27. Yan, D.Y.; Talbot, A.; Nourmohammadi, N.; Cheng, X.Q.; Canady, J.; Sherman, J.; Keidar, M. Principles of using Cold Atmospheric Plasma Stimulated Media for Cancer Treatment. *Sci. Rep.* **2015**, *5*, 17. [CrossRef]
28. Adachi, T.; Tanaka, H.; Nonomura, S.; Hara, H.; Kondo, S.; Hod, M. Plasma-activated medium induces A549 cell injury via a spiral apoptotic cascade involving the mitochondrial-nuclear network. *Free Radic. Biol. Med.* **2015**, *79*, 28–44. [CrossRef]
29. Adachi, T.; Nonomura, S.; Horiba, M.; Hirayama, T.; Kamiya, T.; Nagasawa, H.; Hara, H. Iron stimulates plasma-activated medium-induced A549 cell injury. *Sci. Rep.* **2016**, *6*, 12. [CrossRef]
30. Judee, F.; Fongia, C.; Ducommun, B.; Yousfi, M.; Lobjois, V.; Merbahi, N. Short and long time effects of low temperature Plasma Activated Media on 3D multicellular tumor spheroids. *Sci. Rep.* **2016**, *6*, 12. [CrossRef]
31. Yokoyama, M.; Johkura, K.; Sato, T. Gene expression responses of HeLa cells to chemical species generated by an atmospheric plasma flow. *Biochem. Biophys. Res. Commun.* **2014**, *450*, 1266–1271. [CrossRef] [PubMed]
32. Yan, D.Y.; Lin, L.; Sherman, J.H.; Canady, J.; Trink, B.; Keidar, M. The Correlation Between the Cytotoxicity of Cold Atmospheric Plasma and the Extracellular H_2O_2-Scavenging Rate. *IEEE Trans. Radiat. Plasma Med. Sci.* **2018**, *2*, 618–623. [CrossRef]
33. Antunes, F.; Cadenas, E. Cellular titration of apoptosis with steady state concentrations of H_2O_2: Submicromolar levels of H_2O_2 induce apoptosis through Fenton chemistry independent of the cellular thiol state. *Free Radic. Biol. Med.* **2001**, *30*, 1008–1018. [CrossRef]
34. Klingelhoeffer, C.; Kammerer, U.; Koospal, M.; Muhling, B.; Schneider, M.; Kapp, M.; Kubler, A.; Germer, C.T.; Otto, C. Natural resistance to ascorbic acid induced oxidative stress is mainly mediated by catalase activity in human cancer cells and catalase-silencing sensitizes to oxidative stress. *BMC Complement. Altern. Med.* **2012**, *12*, 10. [CrossRef]
35. Sestili, P.; Brandi, G.; Brambilla, L.; Cattabeni, F.; Cantoni, O. Hydrogen peroxide mediates the killing of U937 tumor cells elicited by pharmacologically attainable concentrations of ascorbic acid: Cell death prevention by extracellular catalase or catalase from cocultured erythrocytes or fibroblasts. *J. Pharmacol. Exp. Ther.* **1996**, *277*, 1719–1725.
36. Verrax, J.; Calderon, P.B. Pharmacologic concentrations of ascorbate are achieved by parenteral administration and exhibit antitumoral effects. *Free Radic. Biol. Med.* **2009**, *47*, 32–40. [CrossRef]
37. Lukes, P.; Dolezalova, E.; Sisrova, I.; Clupek, M. Aqueous-phase chemistry and bactericidal effects from an air discharge plasma in contact with water: Evidence for the formation of peroxynitrite through a pseudo-second-order post-discharge reaction of H_2O_2 and HNO_2. *Plasma Sources Sci. Technol.* **2014**, *23*, 15. [CrossRef]
38. Privat-Maldonado, A.; Gorbanev, Y.; Dewilde, S.; Smits, E.; Bogaerts, A. Reduction of human glioblastoma spheroids using cold atmospheric plasma: The combined effect of short- and long-lived reactive species. *Cancers* **2018**, *10*, 394. [CrossRef]
39. Almasalmeh, A.; Krenc, D.; Wu, B.H.; Beitz, E. Structural determinants of the hydrogen peroxide permeability of aquaporins. *FEBS J.* **2014**, *281*, 647–656. [CrossRef]
40. Bienert, G.P.; Chaumont, F. Aquaporin-facilitated transmembrane diffusion of hydrogen peroxide. *Biochim. Biophys. Acta Gen. Subj.* **2014**, *1840*, 1596–1604. [CrossRef] [PubMed]
41. Miller, E.W.; Dickinson, B.C.; Chang, C.J. Aquaporin-3 mediates hydrogen peroxide uptake to regulate downstream intracellular signaling. *Proc. Natl. Acad. Sci. USA* **2010**, *107*, 15681–15686. [CrossRef] [PubMed]
42. Yusupov, M.; Razzokov, J.; Cordeiro, R.M.; Bogaerts, A. Transport of Reactive Oxygen and Nitrogen Species across Aquaporin: A Molecular Level Picture. *Oxidative Med. Cell. Longev.* **2019**, *2019*, 2930504. [CrossRef]
43. Verkman, A.S.; Hara-Chikuma, M.; Papadopoulos, M.C. Aquaporins–New players in cancer biology. *J. Mol. Med.* **2008**, *86*, 523–529. [CrossRef] [PubMed]
44. Papadopoulos, M.C.; Saadoun, S. Key roles of aquaporins in tumor biology. *Biochim. Biophys. Acta Biomembr.* **2015**, *1848*, 2576–2583. [CrossRef] [PubMed]
45. Erudaitius, D.; Huang, A.; Kazmi, S.; Buettner, G.R.; Rodgers, V.G.J. Peroxiporin Expression Is an Important Factor for Cancer Cell Susceptibility to Therapeutic H_2O_2: Implications for Pharmacological Ascorbate Therapy. *PLoS ONE* **2017**, *12*, e0170442. [CrossRef] [PubMed]
46. Yan, D.Y.; Xiao, H.J.; Zhu, W.; Nourmohammadi, N.; Zhang, L.G.; Bian, K.; Keidar, M. The role of aquaporins in the anti-glioblastoma capacity of the cold plasma-stimulated medium. *J. Phys. D Appl. Phys.* **2017**, *50*, 8. [CrossRef]
47. Makino, N.; Mochizuki, Y.; Bannai, S.; Sugita, Y. Kinetic-studies on the removal of extracellular hydrogen-peroxide by cultured fibroblasts. *J. Biol. Chem.* **1994**, *269*, 1020–1025. [CrossRef]
48. Makino, N.; Sasaki, K.; Hashida, K.; Sakakura, Y. A metabolic model describing the H_2O_2 elimination by mammalian cells including H_2O_2 permeation through cytoplasmic and peroxisomal membranes: Comparison with experimental data. *Biochim. Biophys. Acta Gen. Subj.* **2004**, *1673*, 149–159. [CrossRef]
49. Sasaki, K.; Bannai, S.; Makino, N. Kinetics of hydrogen peroxide elimination by human umbilical vein endothelial cells in culture. *Biochim. Biophys. Acta Gen. Subj.* **1998**, *1380*, 275–288. [CrossRef]
50. Johnson, R.M.; Ho, Y.S.; Yu, D.Y.; Kuypers, F.A.; Ravindranath, Y.; Goyette, G.W. The effects of disruption of genes for peroxiredoxin-2, glutathione peroxidase-1, and catalase on erythrocyte oxidative metabolism. *Free Radic. Biol. Med.* **2010**, *48*, 519–525. [CrossRef]

51. Mueller, S.; Riedel, H.D.; Stremmel, W. Direct evidence for catalase as the predominant H_2O_2-removing enzyme in human erythrocytes. *Blood* **1997**, *90*, 4973–4978. [CrossRef]
52. Winterbourn, C.C.; Stern, A. Human red-cells scavenge extracellular hydrogen-peroxide and inhibit formation of hypochlorous acid and hydroxyl radical. *J. Clin. Investig.* **1987**, *80*, 1486–1491. [CrossRef]
53. Baker, A.M.; Oberley, L.W.; Cohen, M.B. Expression of antioxidant enzymes in human prostatic adenocarcinoma. *Prostate* **1997**, *32*, 229–233. [CrossRef]
54. Beck, R.; Pedrosa, R.C.; Dejeans, N.; Glorieux, C.; Leveque, P.; Gallez, B.; Taper, H.; Eeckhoudt, S.; Knoops, L.; Calderon, P.B.; et al. Ascorbate/menadione-induced oxidative stress kills cancer cells that express normal or mutated forms of the oncogenic protein Bcr-Abl. An in vitro and in vivo mechanistic study. *Investig. New Drugs* **2011**, *29*, 891–900. [CrossRef] [PubMed]
55. Bostwick, D.G.; Alexander, E.E.; Singh, R.; Shan, A.; Qian, J.Q.; Santella, R.M.; Oberley, L.W.; Yan, T.; Zhong, W.X.; Jiang, X.H.; et al. Antioxidant enzyme expression and reactive oxygen species damage in prostatic intraepithelial neoplasia and cancer. *Cancer* **2000**, *89*, 123–134. [CrossRef]
56. Ho, J.C.M.; Zheng, S.; Comhair, S.A.A.; Farver, C.; Erzurum, S.C. Differential expression of manganese superoxide dismutase and catalase in lung cancer. *Cancer Res.* **2001**, *61*, 8578–8585.
57. Kwei, K.A.; Finch, J.S.; Thompson, E.J.; Bowden, G.T. Transcriptional repression of catalase in mouse skin tumor progression. *Neoplasia* **2004**, *6*, 440–448. [CrossRef] [PubMed]
58. Lauer, C.; Volkl, A.; Riedl, S.; Fahimi, H.D.; Beier, K. Impairment of peroxisomal biogenesis in human colon carcinoma. *Carcinogenesis* **1999**, *20*, 985–989. [CrossRef] [PubMed]
59. Glorieux, C.; Sandoval, J.M.; Fattaccioli, A.; Dejeans, N.; Garbe, J.C.; Dieu, M.; Verrax, J.; Renard, P.; Huang, P.; Calderon, P.B. Chromatin remodeling regulates catalase expression during cancer cells adaptation to chronic oxidative stress. *Free Radic. Biol. Med.* **2016**, *99*, 436–450. [CrossRef]
60. Sato, K.; Ito, K.; Kohara, H.; Yamaguchi, Y.; Adachi, K.; Endo, H. Negative regulation of catalase gene-expression in hepatoma-cells. *Mol. Cell. Biol.* **1992**, *12*, 2525–2533. [CrossRef]
61. Guner, G.; Kokoglu, E.; Guner, A. Hydrogen-peroxide detoxication by catalase in subcellular-fractions of human-brain tumors and normal brain-tissues. *Cancer Lett.* **1985**, *27*, 221–224. [CrossRef]
62. Doskey, C.M.; Buranasudja, V.; Wagner, B.A.; Wilkes, J.G.; Du, J.; Cullen, J.J.; Buettner, G.R. Tumor cells have decreased ability to metabolize H_2O_2: Implications for pharmacological ascorbate in cancer therapy. *Redox Biol.* **2016**, *10*, 274–284. [CrossRef]
63. Marklund, S.L.; Westman, N.G.; Lundgren, E.; Roos, G. Copper-containing and zinc-containing superoxide-dismutase, manganese-containing superoxide-dismutase, catalase, and glutathione-peroxidase in normal and neoplastic human cell-lines and normal human-tissues. *Cancer Res.* **1982**, *42*, 1955–1961. [PubMed]
64. Gebicka, L.; Didik, J. Catalytic scavenging of peroxynitrite by catalase. *J. Inorg. Biochem.* **2009**, *103*, 1375–1379. [CrossRef]
65. Alvarez, B.; Radi, R. Peroxynitrite reactivity with amino acids and proteins. *Amino Acids* **2003**, *25*, 295–311. [CrossRef] [PubMed]
66. Augusto, O.; Goldstein, S.; Hurst, J.K.; Lind, J.; Lymar, S.V.; Merenyi, G.; Radi, R. Carbon dioxide-catalyzed peroxynitrite reactivity–The resilience of the radical mechanism after two decades of research. *Free Radic. Biol. Med.* **2019**, *135*, 210–215. [CrossRef]
67. Carballal, S.; Bartesaghi, S.; Radi, R. Kinetic and mechanistic considerations to assess the biological fate of peroxynitrite. *Biochim. Biophys. Acta Gen. Subj.* **2014**, *1840*, 768–780. [CrossRef]
68. Radi, R. Peroxynitrite, a Stealthy Biological Oxidant. *J. Biol. Chem.* **2013**, *288*, 26464–26472. [CrossRef]
69. Squadrito, G.L.; Pryor, W.A. Oxidative chemistry of nitric oxide: The roles of superoxide, peroxynitrite, and carbon dioxide. *Free Radic. Biol. Med.* **1998**, *25*, 392–403. [CrossRef]
70. Rong, L.; Zhang, C.; Lei, Q.; Hu, M.M.; Feng, J.; Shu, H.B.; Liu, Y.; Zhang, X.Z. Hydrogen peroxide detection with high specificity in living cells and inflamed tissues. *Regen. Biomater.* **2016**, *3*, 217–222. [CrossRef]
71. Ermakova, Y.G.; Bilan, D.S.; Matlashov, M.E.; Mishina, N.M.; Markvicheva, K.N.; Subach, O.M.; Subach, F.V.; Bogeski, I.; Hoth, M.; Enikolopov, G.; et al. Red fluorescent genetically encoded indicator for intracellular hydrogen peroxide. *Nat. Commun.* **2014**, *5*, 9. [CrossRef]
72. Enyedi, B.; Zana, M.; Donko, A.; Geiszt, M. Spatial and Temporal Analysis of NADPH Oxidase-Generated Hydrogen Peroxide Signals by Novel Fluorescent Reporter Proteins. *Antioxid. Redox Signal.* **2013**, *19*, 523–534. [CrossRef] [PubMed]
73. Nathan, C.F.; Silverstein, S.C.; Brukner, L.H.; Cohn, Z.A. Extracellular cytolysis by activated macrophages and granulocytes. 2. hydrogen-peroxide as a mediator of cytotoxicity. *J. Exp. Med.* **1979**, *149*, 100–113. [CrossRef]
74. Roos, D.; Weening, R.S.; Voetman, A.A.; Vanschaik, M.L.J.; Bot, A.A.M.; Meerhof, L.J.; Loos, J.A. Protection of phagocytic leukocytes by endogenous glutathione–studies in a family with glutathione-reductase deficiency. *Blood* **1979**, *53*, 851–866. [CrossRef] [PubMed]
75. Roos, D.; Weening, R.S.; Wyss, S.R.; Aebi, H.E. Protection of human-neutrophils by endogenous catalase–studies with cells from catalase-deficient individuals. *J. Clin. Investig.* **1980**, *65*, 1515–1522. [CrossRef] [PubMed]
76. Abe, M.K.; Chao, T.S.O.; Solway, J.; Rosner, M.R.; Hershenson, M.B. Hydrogen-peroxide stimulates mitogen-activated protein-kinase in bovine tracheal myocytes-implications for human airway disease. *Am. J. Respir. Cell Mol. Biol.* **1994**, *11*, 577–585. [CrossRef] [PubMed]
77. Bae, G.U.; Seo, D.W.; Kwon, H.K.; Lee, H.Y.; Hong, S.; Lee, Z.W.; Ha, K.S.; Lee, H.W.; Han, J.W. Hydrogen peroxide activates p70(S6k) signaling pathway. *J. Biol. Chem.* **1999**, *274*, 32596–32602. [CrossRef]

78. Milligan, S.A.; Owens, M.W.; Grisham, M.B. Differential regulation of extracellular signal-regulated kinase and nuclear factor-kappa B signal transduction pathways by hydrogen peroxide and tumor necrosis factor. *Arch. Biochem. Biophys.* **1998**, *352*, 255–262. [CrossRef] [PubMed]
79. Muller, J.M.; Cahill, M.A.; Rupec, R.A.; Baeuerle, P.A.; Nordheim, A. Antioxidants as well as oxidants activate c-fos via Ras-dependent activation of extracellular-signal-regulated kinase 2 and Elk-1. *Eur. J. Biochem.* **1997**, *244*, 45–52. [CrossRef]
80. Stevenson, M.A.; Pollock, S.S.; Coleman, C.N.; Calderwood, S.K. X-irradiation, phorbol esters, and H_2O_2 stimulate mitogen-activated protein-kinase activity in nih-3t3 cells through the formation of reactive oxygen intermediates. *Cancer Res.* **1994**, *54*, 12–15. [PubMed]
81. Bilsland, E.; Molin, C.; Swaminathan, S.; Ramne, A.; Sunnerhagen, P. Rck1 and Rck2 MAPKAP kinases and the HOG pathway are required for oxidative stress resistance. *Mol. Microbiol.* **2004**, *53*, 1743–1756. [CrossRef] [PubMed]
82. Park, B.G.; Yoo, C.I.; Kim, H.T.; Kwon, C.H.; Kim, Y.K. Role of mitogen-activated protein kinases in hydrogen peroxide-induced cell death in osteoblastic cells. *Toxicology* **2005**, *215*, 115–125. [CrossRef]
83. Staleva, L.; Hall, A.; Orlow, S.J. Oxidative stress activates FUS1 and RLM1 transcription in the yeast Saccharomyces cerevisiae in an oxidant-dependent manner. *Mol. Biol. Cell* **2004**, *15*, 5574–5582. [CrossRef] [PubMed]
84. Denicola, A.; Freeman, B.A.; Trujillo, M.; Radi, R. Peroxynitrite reaction with carbon dioxide/bicarbonate: Kinetics and influence on peroxynitrite-mediated oxidations. *Arch. Biochem. Biophys.* **1996**, *333*, 49–58. [CrossRef]
85. Uppu, R.M.; Squadrito, G.L.; Pryor, W.A. Acceleration of peroxynitrite oxidations by carbon dioxide. *Arch. Biochem. Biophys.* **1996**, *327*, 335–343. [CrossRef] [PubMed]
86. Bonini, M.G.; Radi, R.; Ferrer-Sueta, G.; Ferreira, A.M.D.; Augusto, O. Direct EPR detection of the carbonate radical anion produced from peroxynitrite and carbon dioxide. *J. Biol. Chem.* **1999**, *274*, 10802–10806. [CrossRef] [PubMed]
87. Goldstein, S.; Czapski, G. Viscosity effects on the reaction of peroxynitrite with CO_2: Evidence for radical formation in a solvent cage. *J. Am. Chem. Soc.* **1999**, *121*, 2444–2447. [CrossRef]
88. Hodges, G.R.; Ingold, K.U. Cage-escape of geminate radical pairs can produce peroxynitrate from peroxynitrite under a wide variety of experimental conditions. *J. Am. Chem. Soc.* **1999**, *121*, 10695–10701. [CrossRef]
89. Squadrito, G.L.; Pryor, W.A. Mapping the reaction of peroxynitrite with CO_2: Energetics, reactive species, and biological implications. *Chem. Res. Toxicol.* **2002**, *15*, 885–895. [CrossRef]
90. Gebicka, L.; Didik, J.; Gebicki, J. Reactions of heme proteins with carbonate radical anion. *Res. Chem. Intermed.* **2009**, *35*, 401–409. [CrossRef]
91. Movahed, Z.G.; Rastegari-Pouyani, M.; Mohammadi, M.H.; Mansouri, K. Cancer cells change their glucose metabolism to overcome increased ROS: One step from cancer cell to cancer stem cell? *Biomed. Pharmacother.* **2019**, *112*, 15.
92. Medrano-Fernandez, I.; Bestetti, S.; Bertolotti, M.; Bienert, G.P.; Bottino, C.; Laforenza, U.; Rubartelli, A.; Sitia, R. Stress Regulates Aquaporin-8 Permeability to Impact Cell Growth and Survival. *Antioxid. Redox Signal.* **2016**, *24*, 1031–1044. [CrossRef] [PubMed]
93. Leduc, M.; Guay, D.; Leask, R.L.; Coulombe, S. Cell permeabilization using a non-thermal plasma. *New J. Phys.* **2009**, *11*, 12. [CrossRef]
94. Sasaki, S.; Honda, R.; Hokari, Y.; Takashima, K.; Kanzaki, M.; Kaneko, T. Characterization of plasma-induced cell membrane permeabilization: Focus on OH radical distribution. *J. Phys. D Appl. Phys.* **2016**, *49*, 8. [CrossRef]
95. Chung, T.H.; Stancampiano, A.; Sklias, K.; Gazeli, K.; Andre, F.M.; Dozias, S.; Douat, C.; Pouvesle, J.M.; Sousa, J.S.; Robert, E.; et al. Cell Electropermeabilisation Enhancement by Non-Thermal-Plasma-Treated PBS. *Cancers* **2020**, *12*, 219. [CrossRef] [PubMed]
96. Marla, S.S.; Lee, J.; Groves, J.T. Peroxynitrite rapidly permeates phospholipid membranes. *Proc. Natl. Acad. Sci. USA* **1997**, *94*, 14243–14248. [CrossRef] [PubMed]
97. Kirkman, H.N.; Gaetani, G.F. Catalase–A tetrameric enzyme with 4 tightly bound molecules of nadph. *Proc. Natl. Acad. Sci. USA* **1984**, *81*, 4343–4347. [CrossRef]
98. Kirkman, H.N.; Rolfo, M.; Ferraris, A.M.; Gaetani, G.F. Mechanisms of protection of catalase by NADPH–Kinetics and stoichiometry. *J. Biol. Chem.* **1999**, *274*, 13908–13914. [CrossRef] [PubMed]
99. Ahn, H.J.; Kim, K.I.; Hoan, N.N.; Kim, C.H.; Moon, E.; Choi, K.S.; Yang, S.S.; Lee, J.S. Targeting cancer cells with reactive oxygen and nitrogen species generated by atmospheric-pressure air plasma. *PLoS ONE* **2014**, *9*, e86173. [CrossRef] [PubMed]
100. Hirst, A.M.; Simms, M.S.; Mann, V.M.; Maitland, N.J.; O'Connell, D.; Frame, F.M. Low-temperature plasma treatment induces DNA damage leading to necrotic cell death in primary prostate epithelial cells. *Br. J. Cancer* **2015**, *112*, 1536–1545. [CrossRef]
101. Mohades, S.; Laroussi, M.; Sears, J.; Barekzi, N.; Razavi, H. Evaluation of the effects of a plasma activated medium on cancer cells. *Phys. Plasmas* **2015**, *22*, 6. [CrossRef]
102. Yang, H.; Lu, R.; Xian, Y.; Gan, L.; Lu, X.; Yang, X. Effects of atmospheric pressure cold plasma on human hepatocarcinoma cell and its 5-fluorouracil resistant cell line. *Phys. Plasmas* **2015**, *22*, 9. [CrossRef]
103. Chance, B.; Sies, H.; Boveris, A. Hydroperoxide metabolism in mammalian organs. *Physiol. Rev.* **1979**, *59*, 527–605. [CrossRef] [PubMed]
104. Kissner, R.; Nauser, T.; Bugnon, P.; Lye, P.G.; Koppenol, W.H. Formation and properties of peroxynitrite as studied by laser flash photolysis, high-pressure stopped-flow technique, and pulse radiolysis. *Chem. Res. Toxicol.* **1997**, *10*, 1285–1292. [CrossRef]
105. Pryor, W.A.; Squadrito, G.L. The chemistry of peroxynitrite—A product from the reaction of nitric-oxide with superoxide. *Am. J. Physiol. Lung Cell. Mol. Physiol.* **1995**, *268*, L699–L722. [CrossRef] [PubMed]
106. Gutman, M.; Nachliel, E. The dynamic aspects of proton-transfer processes. *Biochim. Biophys. Acta* **1990**, *1015*, 391–414. [CrossRef]

107. Samouilov, A.; Woldman, Y.Y.; Zweier, J.L.; Khramtsov, V.V. Magnetic resonance study of the transmembrane nitrite diffusion. *Nitric Oxide Biol. Chem.* **2007**, *16*, 362–370. [CrossRef]
108. May, J.M.; Qu, Z.C.; Xia, L.; Cobb, C.E. Nitrite uptake and metabolism and oxidant stress in human erythrocytes. *Am. J. Physiol. Cell Physiol.* **2000**, *279*, C1946–C1954. [CrossRef]
109. Denicola, A.; Souza, J.M.; Radi, R. Diffusion of peroxynitrite across erythrocyte membranes. *Proc. Natl. Acad. Sci. USA* **1998**, *95*, 3566–3571. [CrossRef] [PubMed]
110. Jordanoglou, J.; Tatsis, G.; Danos, J.; Gougoulakis, S.; Orfanidou, D.; Gaga, M. Alveolar partial pressures of carbon-dioxide and oxygen measured by a helium washout technique. *Thorax* **1990**, *45*, 520–524. [CrossRef]
111. Gaston, B.; Reilly, J.; Drazen, J.M.; Fackler, J.; Ramdev, P.; Arnelle, D.; Mullins, M.E.; Sugarbaker, D.J.; Chee, C.; Singel, D.J.; et al. Endogenous nitrogen-oxides and bronchodilator s-nitrosothiols in human airways. *Proc. Natl. Acad. Sci. USA* **1993**, *90*, 10957–10961. [CrossRef] [PubMed]
112. Green, L.C.; Wagner, D.A.; Glogowski, J.; Skipper, P.L.; Wishnok, J.S.; Tannenbaum, S.R. Analysis of nitrate, nitrite, and n-15 -labeled nitrate in biological-fluids. *Anal. Biochem.* **1982**, *126*, 131–138. [CrossRef]
113. Leone, A.M.; Francis, P.L.; Rhodes, P.; Moncada, S. A rapid and simple method for the measurement of nitrite and nitrate in plasma by high-performance capillary electrophoresis. *Biochem. Biophys. Res. Commun.* **1994**, *200*, 951–957. [CrossRef] [PubMed]
114. Jones, D.P. Radical-free biology of oxidative stress. *Am. J. Physiol. Cell Physiol.* **2008**, *295*, C849–C868. [CrossRef] [PubMed]
115. Adimora, N.J.; Jones, D.P.; Kemp, M.L. A model of redox kinetics implicates the thiol proteome in cellular hydrogen peroxide responses. *Antioxid. Redox Signal.* **2010**, *13*, 731–743. [CrossRef]
116. Oshino, N.; Chance, B.; Sies, H.; Bucher, T. Role of H_2O_2 generation in perfused rat-liver and reaction of catalase compound 1 and hydrogen donors. *Arch. Biochem. Biophys.* **1973**, *154*, 117–131. [CrossRef]
117. Puck, T.T.; Marcus, P.I.; Cieciura, S.J. Clonal growth of mammalian cells invitro-growth characteristics of colonies from single hela cells with and without a feeder layer. *J. Exp. Med.* **1956**, *103*, 273–283. [CrossRef]